UNIVERSIDAD DE CHILE
FACULTAD DE CIENCIAS FISICAS Y MATEMÁTICAS
DEPARTAMENTO DE INGENIERIA DE MINAS

QUANTIFYING THE INFLUENCE OF GEOLOGICAL FAULTS ON THE STABILITY OF OPEN STOPES' BACK WALLS

TESIS PARA OPTAR AL GRADO DE MAGISTER EN MINERÍA

JEAN LOUIS AZORIN FLORES

PROFESOR GUÍA:
JAVIER VALLEJOS MASSA

PROFESOR CO-GUÍA:
ROBERTO JESUS MIRANDA CONTRERAS

MIEMBROS DE LA COMISIÓN:

RODRIGO ORTIZ BORGOÑO
LUIS FELIPE ORELLANA ESPINOZA
KIMIE ELIANA SUZUKI MORALES

SANTIAGO DE CHILE
2022

RESUMEN DE LA TESIS PARA OPTAR AL GRADO DE: Magíster en Minería
POR: Jean Louis Azorin Flores
FECHA: 2022
PROFESOR GUÍA: Javier Vallejos Massa

CUANTIFICANDO LA INFLUENCIA DE FALLAS GEOLÓGICAS EN LA ESTABILIDAD DE TECHOS DE CASERONES ABIERTOS

El método de gráfico de estabilidad de Mathews es usado ampliamente para el diseño de minas subterráneas de caserones abiertos. Como método empírico, utiliza variables de entrada como la calidad del macizo rocoso y factores de ajuste que representan el impacto en la estabilidad de varios parámetros. El método de Mathews tiene varias limitaciones, entre ellas la imposibilidad de representar la influencia de las fallas en la integridad del caserón.

Este estudio propone dos métodos para la inclusión de fallas en el análisis de estabilidad para el diseño de caserones como factor de ajuste del número de estabilidad. La primera forma es utilizar la orientación de la falla en el gráfico de valores de factor B. El segundo método consiste en crear un nuevo factor de ajuste F para cuantificar la influencia de las fallas en la estabilidad de la pared trasera del rebaje.

Para producir los resultados necesarios para el cálculo del factor de ajuste F se utilizó modelado numérico 3D. Se proponen dos formas de cálculo del factor F, ambas utilizando los volúmenes de sobre excavación obtenidos en los modelos numéricos. Se incluyeron varias configuraciones de orientación de fallas relativa al caserón en los gráficos de factor F, que incluyen tres diferentes strikes y cinco diferentes dips, así como dos posiciones de intersección para los casos de fallas paralelas y cinco distancias entre la falla y el techo del caserón para el caso de fallas horizontales.

Los resultados muestran que el strike juega un papel importante en la influencia que tiene una falla sobre la estabilidad del techo de un caserón. El strike paralelo tiene el mayor impacto. En tal caso, el manteo de la falla tiene poca importancia ya que todos los resultados muestran un gran volumen de sobre excavación generado por la falla.

El punto de intersección del techo del caserón y la falla es relevante para el análisis de estabilidad. Las fallas que cruzan el techo del caserón cerca del “borde lejano”; vale decir, el borde opuesto a la dirección de manteo de la falla, producen mayor sobre excavación. El impacto de la falla en la estabilidad del caserón disminuye a medida que aumenta la distancia entre el punto de intersección y el borde cercano del techo del caserón.

Si la falla es horizontal, la distancia entre la falla y el techo del caserón es de gran importancia. Los resultados sugieren que existe una distancia crítica que maximiza el volumen de sobre excavación producido por la falla. Si se supera esta distancia, la influencia de la falla en la estabilidad del techo del caserón disminuye rápidamente hasta no tener ninguna influencia. Como solo se utilizó un conjunto de parámetros del macizo rocoso para todos los modelos numéricos, se presume que esta distancia crítica depende, entre otras cosas, de la resistencia del macizo rocoso.

THIS THESIS IS SUBMITTED FOR
THE DEGREE OF: Master in Mining
BY: Jean Louis Azorin Flores
DATE: 2022
ADVISOR: Javier Vallejos Massa

QUANTIFYING THE INFLUENCE OF GEOLOGICAL FAULTS ON THE STABILITY OF OPEN STOPES' BACK WALLS

Mathews' stability graph method is widely used for open stope mine design. As an empirical method, it relies on inputs such as rock mass quality and adjustment factors accounting for the impact of key parameters on stability. Mathews' method has several limitations, among them the impossibility of representing the influence of discrete faults on stope integrity.

This study proposes two methods for the inclusion of faults in the stability analysis for stope design as an adjusting factor of the stability number. The first way is to use the fault orientation in the B factor chart. The second method is to create a new adjustment factor, "F", to quantify the influence of faults in the stope back stability.

3D numerical modelling was used to produce the results for the calculation of the adjustment factor F. Two ways of calculation of the F factor are proposed, both using the overbreak volumes obtained in the numerical models. Several stope-fault orientation configurations were included in the F factor charts including three different fault strikes and five different dips as well as two intersecting positions for the parallel strike cases and five different distances from the stope back, for the case of horizontal faults.

Results show that strike plays a major role on the influence a fault has over the stability of the stope back. Parallel strike has the greatest impact. In such case, fault's dip is of little importance as all outcomes show great overbreak volumes attributed to the fault.

The point of intersection between the fault and the stope back is also relevant for the stability analysis. Faults intersecting the stope back at its "far edge"; that is, the edge towards the fault dip direction, is the worst-case scenario. The fault's impact decreases as the distance between the line of intersection moves towards the stope center.

If the fault is horizontal, the distance between the fault and the stope back is of great importance. Results suggest that there is a critical distance that maximizes the overbreak volume produced by the fault. If this distance is surpassed, the fault's influence on the stope back quickly diminishes until it has no influence at all. As only one set of rock mass parameters was used for the all the numerical models, it is presumed that this critical distance is dependent, among other things, on the rock mass strength.

To whoever cares about this subject.

Acknowledgments

The authors acknowledge the financial support from the basal CONICYT project (grant) AFB180004 of the Advanced Mining Technology Center (AMTC) – University of Chile and FONDEF proyect (grant) IT17M10005 - MINEROC, plataforma tecnológica para el diseño en la mediana minería subterránea.

Contents

Index of Figures

Index of tables

Chapter 1 Introduction

1.1 General Introduction

The stability of rock mass surrounding excavations is of paramount importance for underground mining activities. Mineral extraction is done in large stopes which dimensions must be optimized considering not only economical perspectives but also stope integrity during the mining process.

For the past three decades, the graphical method originally introduced by Mathews (1980) has been used as an empirical tool for designing and assessing the stability performance of open stopes. Through this method, the stability performance of excavations' surfaces (walls) is compared to an empirically generated database and is plotted in Mathews' stability graph.

The stability graph is generally used as a design tool for underground mines using the sublevel stoping (SLS) method, which is selective and seeks to minimize dilution. However, stope walls instability can generate the slough of unwanted materials into the excavation (dilution) resulting in, among other things, poor blend grade.

Despite being widely used in the industry, mainly because of its simplicity, Mathews' stability graph method has several limitations:

- The results are mainly qualitative as the method has no way of quantifying the damage or dilution of the excavation surface.

- The method requires geometrical simplification of sometimes complex stope shapes.

- There is no built-in way of estimating the influence of closely located excavations as in an array of several stopes (ie. transverse stoping).

- It assumes the same rock mass conditions for the whole extension of the stope as it assigns a single stability number N to each stope surface, disregarding the variability of the rock mass.

- The possibility of using backfill is not contemplated in the stability number N, excluding it from the stability assessment.

- As it uses the modified NGI-Q index, Mathews' method does not consider the impact of underground water on stope performance, even thought it is known to have a negative impact.

- The original graph was developed by Mathews using 50 case histories. However, most of these cases were obtained from excavation of relatively small dimensions, with hydraulic radii ranging from 2 to 15 meters, in steeply dipping ore bodies. A majority of the case histories of the original database were excavations made in medium to good quality rock mass at a depth of over 1000 meters.

- In highly fractured rock masses, such as those common in northern Chile, the presence of two or more sub-vertically oriented joint sets, as well a at least one sub-horizontal one, is not unusual. Given the method by which it is derived, low values of the B factor are common, often leading to an under estimation of the stability number N with respect to documented performance. Additionally, even though the structural factor B considers a minimum value for spacing and persistence of joints, this information is not used for the calculation of B.

- Mathews' method does not account for the influence of faults on stope stability. Geological faults are known to be detrimental for excavation stability as they can cause severe overbreak and compromise the stability of the stope.

This study engages the latter limitation and seeks to present alternatives to quantitatively introduce the impact of geological faults in the graphical method for stope design.

1.2 Objetives of the Thesis

1.2.1 General Objective

This study seeks to evaluate the influence of geological faults on the stability of stopes in a quantitative fashion in the scope of Mathews' stability graph method.

1.2.2 Specific objectives

- To generate a stability boundary for a given database using fault orientation to calculater the B factor that is used to calculate the stability number.

- To compare the quality of the boundaries obtained calculating the B factor using faults and joints (regular B factor).

- To quantify the influence of faults of various orientations over the stability of a stope's back.

- To present a methodology for the calculation of an adjusting factor F which adjust the stability number N by accounting for the impact of faults.

1.3 Scope of the research

- This study was held using the available data from three mines located in the north of Chile. No additional in-situ information was collected for this thesis.

- As not enough empirical information about the effect of faults for different orientation was available, numerical modelling was used to generate the different results used for the calculation of the F facor.

- All numerical models were done in Itasca's three-dimesnional finite difference code FLAC3D v6.0.

1.4 Thesis contents

This thesis is based on papers and is structured in three chapters as shown below:

Chapter 1: The general theme of the thesis is presented, including the problems to be addressed, general and specific objectives, scope and the state of the art.

Chapter 2: The methodology used to obtain the results presented in chapter 3.

Chapter 3: This chapter presents the results and analysis contained in the papers. As the thesis is based on two papers, this chapter is devided in two parts:

- Results from: *Use of B factor from major geological faults' orientation on Mathews' stability graph method. A case study.*
- Results from: F factor: *Quantifying the impact of faults on open stope's back stability.*

Chapter 4: All the relevant findings of the research for both papers are presented on this chapter. The limitations of the results and recommendations for future works are also included.

Chapter 5: *Bibliography*

1.5 General Background

1.5.1 Sublevel Stoping (SLS)

Underground mining methods with self-supporting open excavations are widely used around the world. Of these methods, sublevel stoping is highly productive due to the large size of the resulting stopes (Zablocki, 2009). It is normally used to mine tabular shaped orebodies such as mineralized veins but can also be used in large, massive orebodies with vertical to sub-vertical dips, usually surrounded by strong host rock masses.

The sublevel stoping method has several advantages such as low costs and high levels of mechanization in drilling and loading operations, which allow the method to achieve high production rates with minimum personnel. There are, however, disadvantages to this method such as the large amount of development and infrastructure necessary to start and maintain production rates.

The success of this mining method depends largely on the stability of the stope walls, which are usually unsupported (Milne et al., 1998). If the host rock mass is competent, the stopes can reach considerable dimensions.

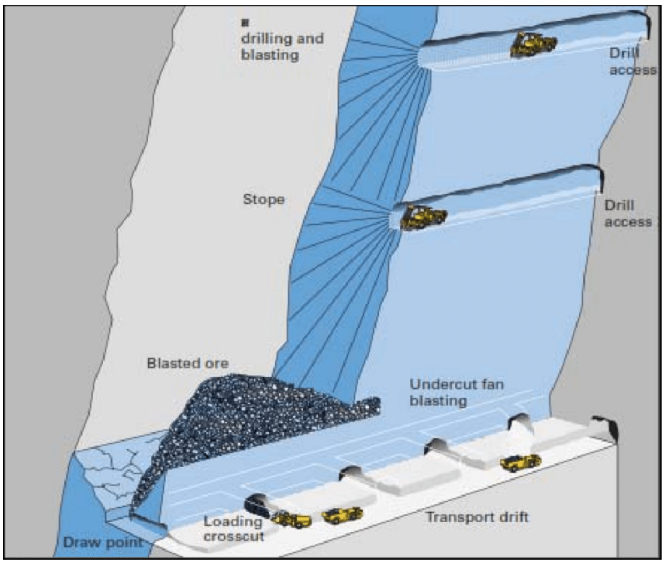

Figure 1 Scheme of Sbulevel Stoping development (Hamrin et al, 2001)

1.5.2 Mathews' stability graph method

Despite its limitations, Mathews' graphical method for stope design is widely used and accepted in the industry. This method assesses the stability performance of individual stope walls by plotting its stability number N versus its hydraulic radius (shape factor) in a semi-logarithmic chart.

The graph has different zones defining different ranges of stability performance. Mathews' original stability graph defines three zones of qualitative performance: a stable zone, a potentially unstable zone and a zone of potential caving, as shown in Figure 2. The stability prediction is defined by the location of the intersection of the wall's stability number N and its hydraulic radius.

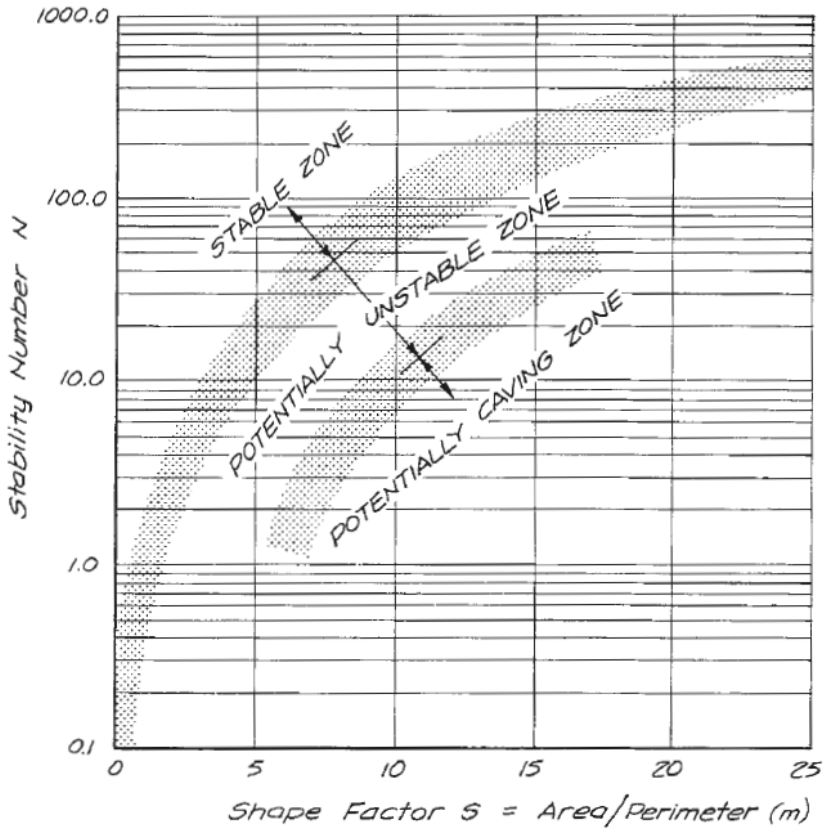

Figure 2 Mathews' stability graph. (Mathews, 1981)

The stability number N is comprised of several inputs and it accounts not only for rock mass quality, but also for induced stresses, structure and geometric influence. It is calculated as shown in equation (1):

$$N = Q' \times A \times B \times C \tag{1}$$

Where Q' is the modified NGI-Q Rock mass classification introduced by Barton (1974), A, B and C are adjusting factors that represent the potential influence of induced stresses, wall and joint set orientation relative to the stope face and gravity effects, respectively. These inputs lie outside the scope of the present work and are therefore not discussed in depth. They are, however, succinctly explained in the following section.

The modified Q value is mainly a measure of the degree of fracturing of a rock mass. It is calculated as follows:

$$Q' = \frac{RQD}{j_n} \times \frac{j_r}{j_a} \tag{2}$$

Where RQD is the rock quality designation (Deere, 1972), Jn is the joint set number, Jr represents the joint roughness and Ja accounts for the degree of alteration.
The calculation is typically separated in two fractions which represent different concepts. The first fraction is a representation of the quantity of fractures in the surrounding rock mass while the second fraction accounts for the general state of the fracture contact

surfaces. While very rough fractures are expected to have a positive impact on stability due to their greater shear strength, highly altered fractures have the opposite effect.

The unmodified Q value has a third component representing the state of stresses on the rock mass, but this is replaced by the A factor in Mathews' graphical method as explained below.

The rock stress factor A accounts for the induced stresses acting on the stope surface in relation to rock strength and is obtained by dividing the maximum induced stress by the uniaxial compressive strength (UCS) of the intact rock. The resulting ratio is input in the graph shown in Figure 3, thereby obtaining the corresponding value of A.

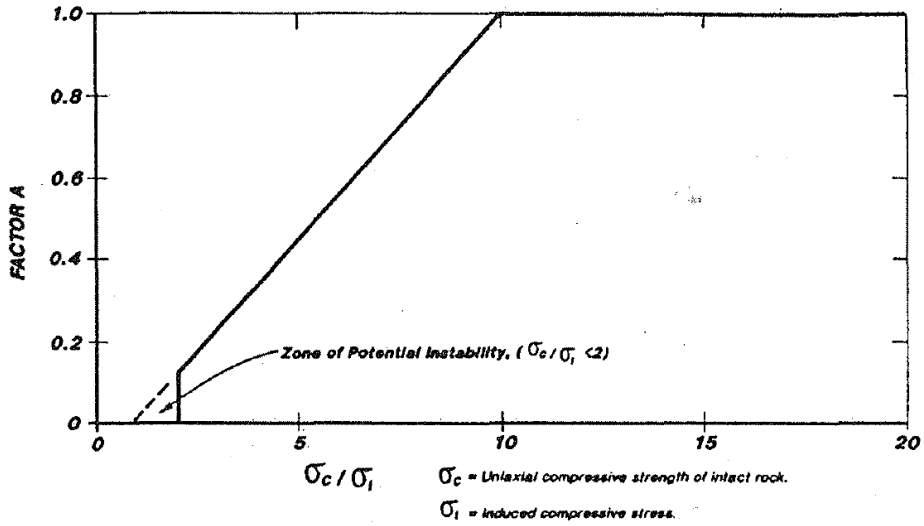

Figure 3 A factor chart. (Stewart & Forsyth, 1993 based on Mathews, 1981)

Ideally, the induced stress values should be obtained from local on-site measurements. However, this is costly and is often not applied to every stope in an underground mine. If on-site measured stress data is not available, elastic numerical modelling can be used to estimate the induced stresses at the stope faces.

If geometrical simplification of the stope can be done, a graphical method developed by Stewart & Forsyth (1993) can be used for estimating the induced stresses at the excavation surface. This method has further simplifications that should be noted: the principal stresses are assumed to be vertical and two perpendicular horizontal that are parallel and normal to the stope face.

The rock stress factor, B, quantifies the influence of joint sets on the stope walls stability. The angle formed between a joint set and the stope face is important as the relative orientation of the two planes has a direct impact on the failure mechanism and the extent of the dilution this failure can generate.

A joint set that is sub-parallel to a stope face can be very detrimental to stability as it allows for easier breaking of rock bridges (the rock located between the joints and the exposed surface), facilitated by blasting damage and deconfinement. These broken rock bridges become loose blocks that can eventually increase the stope's dilution.

If the joint orientation forms a medium to high angle with a stope face, the main failure mechanism becomes sliding along the joint surface and falling into the stope. Rock bridges formed by the joint sets with this relative orientation are less likely to break, resulting in higher values for the B factor.

Perpendicular or sub-perpendicular joint sets relative to the excavation surface are the least detrimental. Compressive stresses acting on the joint surfaces increase frictional strength and reduce the likelihood of instability.

There are several criteria for determining if a joint set is eligible for determining the B factor. These criteria can vary from case to case but as a basic guideline, these should be considered:

- At least three discontinuities of a given set must intersect the excavation surface.
- Potentially unstable blocks formed by the discontinuities and the excavation surface must have a minimum edge length between 1/5 and 1/20 of the maximum excavation span.
- If multiple joint sets meet the criteria, the most critical one (resulting in the lowest B value) is chosen based on persistence and spacing.

The values of B are estimated following the cases shown in Figure 4.

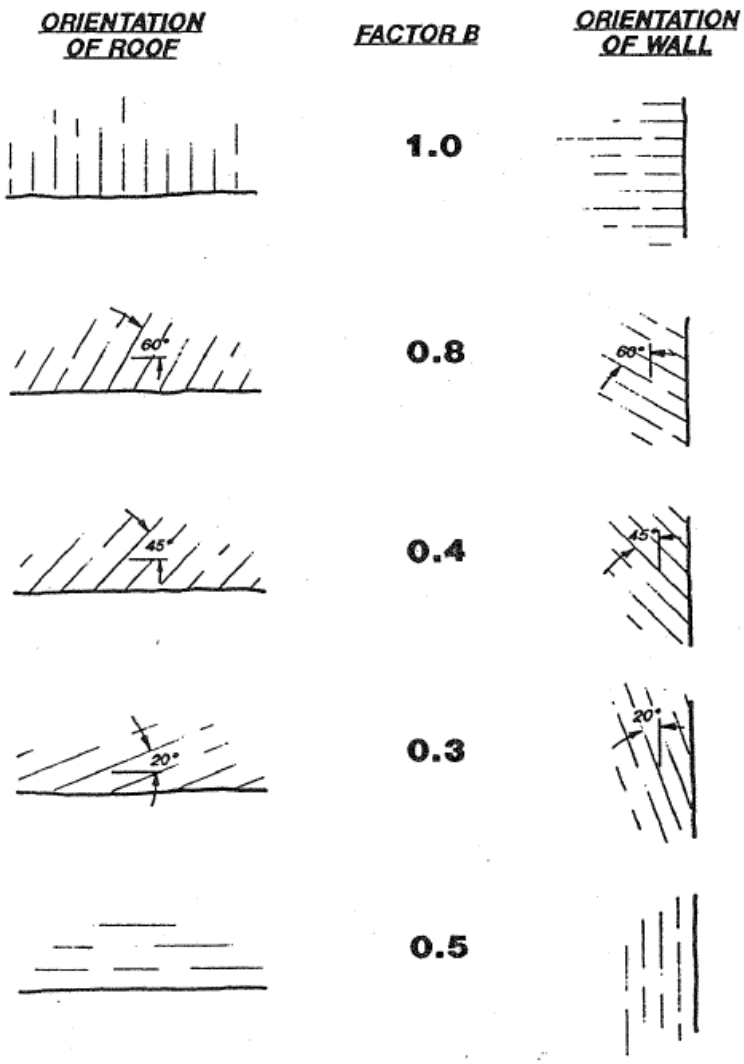

Figure 4 Chart for Estimating the B Factor (Stewart & Forsyth, 1993 based on Mathews, 1981)

The final geotechnical factor, C, accounts for the effects of gravity in the stability of a stope face. This is the simplest one of the three adjusting factors because it has only one input which is the excavation wall inclination. Vertical or steeply dipping walls such as end walls are less likely to produce falling rock blocks than sub-horizontal faces such as the stope back. It must be noted that foot walls can be expected to have the maximum value for C, as rock should not fall from them.

The value of the C factor can be obtained from the graph in Figure 5. The C factor is not always used as a design parameter as, normally, the excavation surface inclination follows the dip of the ore body.

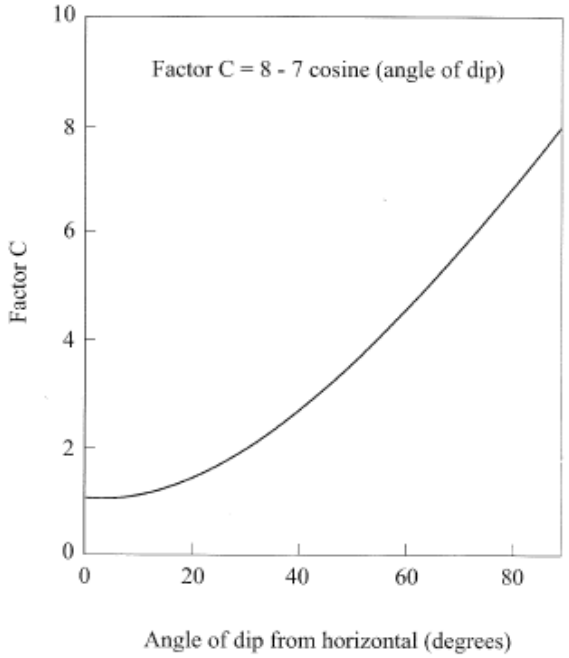

Figure 5 C factor chart (based on Mathews, 1981)

1.5.3 Graphical method over the years

After the compilation of Mathews' original graph method and empirical database, several authors have introduced modifications and additional case histories to expand the graph's database. The authors listed below are by no means the only contributors to the actual state of the graphical method; they are, however, the most relevant for this particular study.

- Potvin et. Al, (1989) proposed a modified stability graph that considered only stable and caved zones based on additional case histories. The new method included modifications to the B and C factors and allowed the use of cable bolt support on the design assessment.

- Nickson (1992) updated the modified stability graph based on additional case histories and introduced graph zones accounting for stable excavation with support and a support transition zone.

- Stewart and Forsyth (1993) not only added more case histories to the original database, but also updated the original graph by introducing new potentially stable, potentially unstable, potential major failure and potential caving zones. The same authors presented a graphical method for estimating the induced stresses based on stope confinement and shape factor, finding widespread adoption for the calculation of the A factor.

- Hadjigerorgiou et al (1995) updated Potvin's modified graph using statistical analysis. This update included modifications to the stable and caving boundary and added a new boundary below which ground support is required. Finally, the

study proposed modifications to the C factor for it to account for failures caused by blocks sliding along joints.

- Clark & Pakalnis (1997) introduced a quantitative version of the stability graph by estimating the unplanned dilution based on equivalent linear overbreak/slough (ELOS) that can be applied to narrow excavations as the stability curves proposed by the authors consider ranges of ELOS going from less than 0.5 m to over 2 m.

- Suorineni (1998) introduced the F factor as an extension to Clark & Pakalnis (1997) ELOS based stability graph. Using 2D numerical modeling, the author evaluated the effects of a fault in the unplanned dilution of narrow, steeply dippin excavations. Several graphs for the determination of the F factor are presented including different geometrical and geomechanical configurations.

- Mawdesley (2003) introduced a significantly larger database of case histories from Trueman et al. (2000) and developed an "extended stability graph" which considered stable, failure and major failure zones in a log-log space by using logistic regression. The author also defined stability contours of isoprobability. The extended stability graph is now widely used in the industry and is understood to be a powerful tool.

- Capes (2009): Similar to Mawdesley (2003) additions to the original stability graph method, Capes updated Clark & Pakalnis (1997) ELOS curves by increasing the case history database and using logistic regression.

- Vallejos et al. (2015) Introduced Mineroc as a computational tool for fast and simple stope stability performance back-analysis.
- Castro (2015) Presented an ELOS based stability chart made using an extended data base including 307 case histories of unsupported open stopes from Canadian mines and 38 from Chilean mines.
- Vallejos et al. (2016) suggested that the use of a modified stress factor A statistically improves the performance of Mathews' stable boundary.

1.5.4 Key Structural Features

This study focuses on the effect of key structural features such as joints and faults on the stability of stopes. It is important to understand some key differences of theses two kind of geological structures.

1.5.4.1 Joints

Fissures of geological origin along which there has been no visible displacement (Brady & Brown, 2013). Joints usually form in groups of similar orientation called joint sets. Joint system forms when multiple joint sets intersect each other. Joint systems produce arrays of rock blocks which in underground mining environment can become "Key Blocks" that can slide and fall into the stopes as overbreak (Goodman & Shi,

1985). Most rock mass contain one or more vertical or highly inclined joint sets (Giekie, 1880) which traduces in a low value of B factor for most stopes' sub-vertical walls.

1.5.4.2 Faults

Fractures on which identifiable shear displacement has taken place (Brady & Brown, 2013). Their thickness varies from millimeters in case of small local faults, to several meters for major regional ones. Faults can be filled with materials such as fault gauge, talc, breccia and other weak minerals. As faults are conceived from relative displacement of two rock volumes, rock walls are often slickensided, thus having very low frictional strength. This is particularly harmful for stopes' walls integrity, as rock block slip and fall may easily occur. In this study faults were provided as solid triangulations. Only mine scale faults were used. If no major fault were to intersect the analyzed stope's walls, a B factor value of one was used.

1.5.5 MineRoc

MineRoc (Vallejos 2015; Vallejos, et al. 2017) is an underground mining software that allows mine planers to define the optimal stope size. This software performs an adaptation of Mathews' stability graph method for a specific mining context, based on local case studies, geology, operational practices, and different stability criteria. This is possible due to the interaction between different modules as shown in Figure 8.

1.5.5.1 Acquisition Module

The required geotechnical information for the stability analysis can be stored in this module. Geotechnical units can store information pertaining to intact rock, rock mass and structural models. Stress fields can be stored as measurements or an overburden model. This information is later used in the Performance or Design modules as inputs to assess previously excavated or newly designed stopes.

The acquisition module can store more information than the other modules need, this allows *MineRoc* to also work as an integrated geotechnical database storage tool.

1.5.5.2 Performance Module

Assessment of a stope's performance is done in this module by means of adding case studies to a back-analysis database. The key feature of this module is the automatic calculation of performance parameters and Mathews' adjustment factors per stope face. The software calculates the area of the walls, the volume of the stope and the overbreak volume (V_{OB}^{wall}, Figure 6) for each individual wall. The overbreak volume is obtained by measuring the volume between a wall from the stope's design and the Cavity Monitoring Survey (CMS) triangulation's limit (Miller, et al. 1992).

MineRoc can obtain either, the volumetric dilution or Equivalent Linear Overbreak Sloughing (ELOS) (Clark & Pakalnis, 1997) per stope face from equations (3) and (4) depending on the user's preferences.

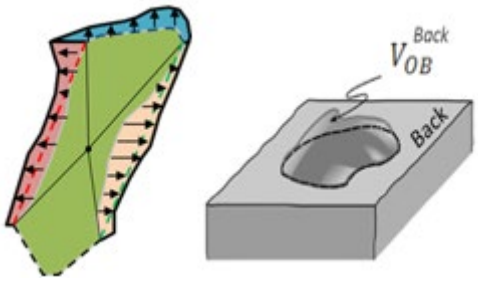

Figure 6 Over break volume interpretation.

$$\text{Vol. Dilution}_{\text{Wall}} = \frac{\text{OverBreak Vol}_{\text{wall}}}{\text{Vol. of the Stope}} \tag{3}$$

$$\text{ELOS} = \frac{\text{OverBreak Vol}_{\text{wall}}}{\text{Area}_{\text{wall}}} \tag{4}$$

Once stope performance is evaluated, *MineRoc* delivers, for each of the stope faces, a stability number *N* based on inputs from the Acquisition module and hydraulic radius alongside other information such as rock mass quality (Q'), wall's orientation (Strike and Dip), individual adjustment factors (A, B and C), over break volume and more.

1.5.5.3 Database Manager Module

Results obtained from the Performance module are stored in the Database Manager. It is possible to compile and partition data between locally analyzed case studies and others found in literature (included as a guide for mines lacking sufficient local case studies) allowing new stability boundaries to be adjusted.

The stability graph is divided in potential stability zones by a logarithmic function curve called the Stability Boundary, which typically has the following form:

$$N = a \cdot RH^b \tag{5}$$

Where *a* and *b* are constants adjusted in order to maximize the Pierce Skill Score (PSS) of the boundary's data classification. For the stability graph method, a stope that is stable and plots above the stability graph boundary is a "true positive" while a stable stope

plotting under this boundary would be a "false negative", and so on. The PSS is obtained as shown below using the "*Confusion Matrix*" in Figure 7 and equations from (6) to (8).

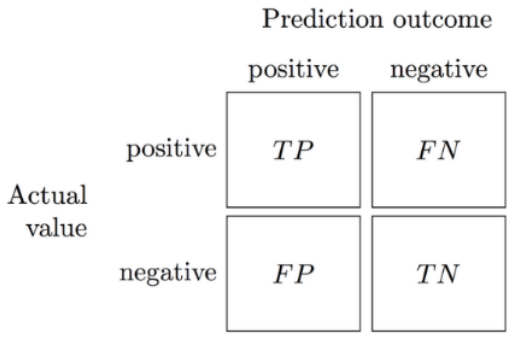

Figure 7 Confusion matrix.

$$TPR = \frac{TP}{P} \tag{6}$$

$$FPR = \frac{FN}{N} \tag{7}$$

$$PSS = TPR - FPR \tag{8}$$

Where TPR is the "true positive ratio", FPR is the "false positive ratio", and PSS is the Pierce Skill Score. PSS ranges from 1 for a perfect classification (every single stable stope wall plotted over the boundary and every unstable one placed below it) to -1 for a "perfectly wrong" classification. In summary, if two curves adjusted using the same acceptability criterion have different PSS values, the one curve with the higher PSS defines a more representative separation of potential stability zones based on the graph's data.

Stability is defined quantitatively by an acceptability criterion which can be defined as an acceptable dilution or ELOS depending on user preference. Multiple boundaries with different acceptability criteria can be adjusted for the same database dividing the graph in potential dilution zones instead of potential stability zones.

1.5.5.4 Stope Design Module

New stope designs are evaluated in this module. Desired stope dimensions, geotechnical units for each face and stress fields are needed in order to plot the potential new stope faces in the stability graph. Once these are plotted, newly adjusted stability boundaries can be loaded to assess the new stope's potential performance.

The stope dimensions are determined based on local geotechnical information, in-situ stress and stability boundaries. Given a set of geotechnical units and a stope face orientation, the design module can calculate the expected stability number N and plot it against the hydraulic radius derived from the input dimensions. The plotted point's location in the stability graph indicates the potential stability of the new design.

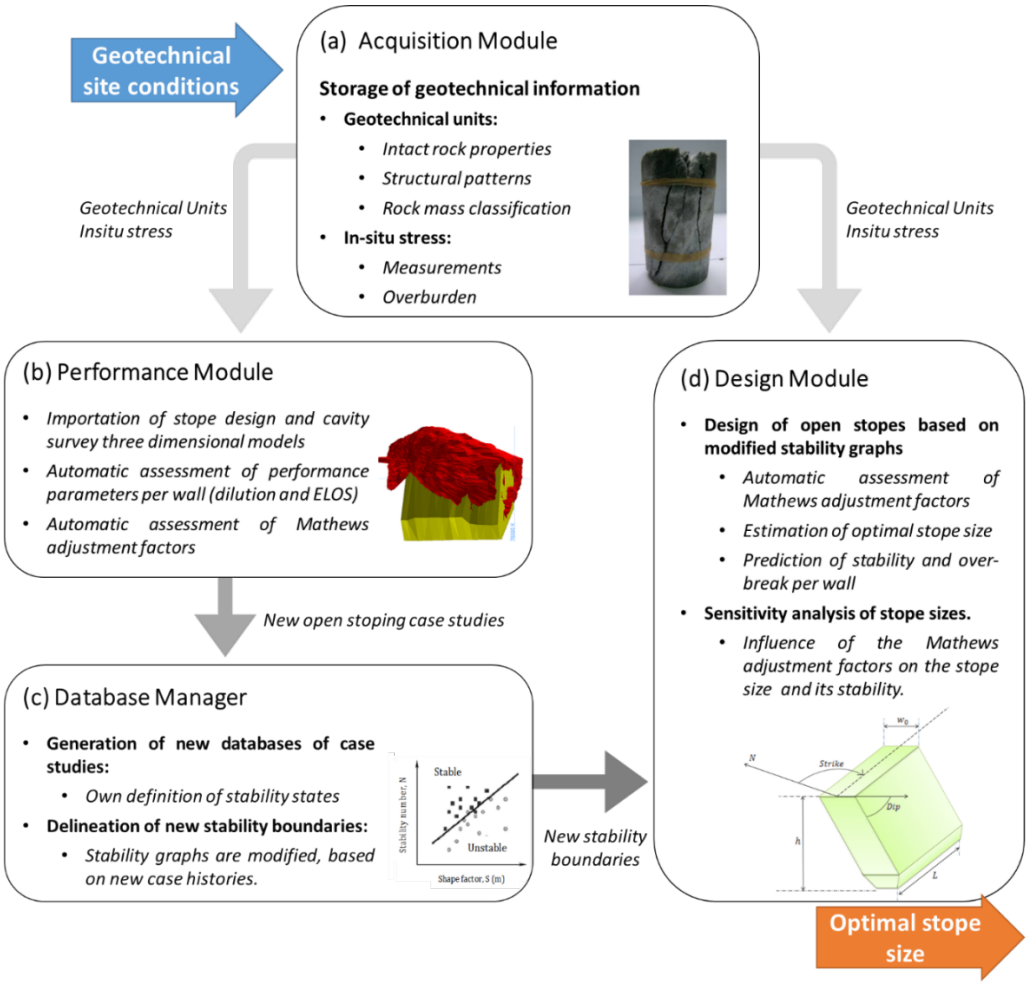

Figure 8 Interaction between modules and information flow in MineRoc

1.5.6 Numerical Modelling

In the past, soil and rock mechanics were considered essentially empirical disciplines. The enormous complexities encountered in natural states of geologic media can make analytical approaches very difficult.

Pioneering work by Karl Terzaghi in the eighties imparted scientific and mathematical bases to many aspects of geotechnical engineering. In these developments, solutions were obtained by means of differential equations that were assumed to govern the physical systems. A number of simplifications and assumptions were necessary to reach a solution.

Although this approach has provided insight for many practical solutions, it cannot yield realistic results for problems involving complex non-homogeneous media, non-linear material behavior, in-situ stress conditions, special variations of material properties, arbitrary geometries, discontinuities and other factors imposed by geologic characteristics.

Newly developing numerical methods can account for many of the mentioned factors and are now widely used in engineering applications.

Most numerical methods require discretization of large, complex problems. In the finite difference method, the basic governing equation is discretized, whereas in the finite element method, the physical continuum is discretized.

Problems in geotechnical engineering can be classified as steady (equilibrium), transient (propagation) and eigenvalue. Table 1 show some of the problems in these categories and their corresponding differential equations.

Table 1 Types of numerical problems in geotechnical engineering. (Modified from C. Desai, 1977)

Problem	Category	Equation
Static stress-deformation analyses for foundations, slopes, tunnels and other structures	Steady	$\frac{\partial^2 u}{\partial x^2} + \frac{\partial^2 u}{\partial y^2} = 0$
Wave propagation	Transient	$\frac{\partial^2 u}{\partial x^2} = \frac{\partial^2 u}{\partial t^2}$
Natural frequencies of foundations and structures	Eigenvalue	$m\frac{\partial^2 u}{\partial t^2} + ku = 0$

In this study, the finite difference method is used. This document will thus exclude further detail on the other numerical methods.

1.5.6.1 Finite Difference Method (FDM)

The discretization procedure is based on replacing continuous derivatives in equations governing the physical problem by the ratio of changed in the variable, over a finite increment as shown in eq. (9) and illustrated by Figure 9.

$$\frac{\partial u}{\partial x} = \lim_{\Delta x \to 0} \frac{\Delta u}{\Delta x} \approx \frac{\Delta u}{\Delta x} \tag{9}$$

As a result of these substitutions, a differential equation is transformed into a difference equation in terms of unknowns at grid points or nodes. The solution of the system equation is obtained after imposing the necessary initial and boundary conditions.

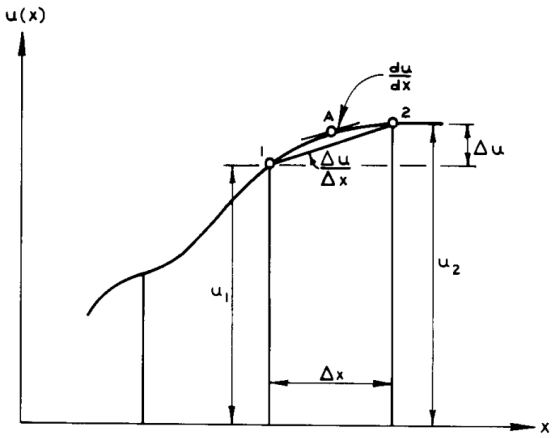

Figure 9 Finite difference approximation to first derivative. (C. Desai, 1997)

The differential equations that need to be approximated involve first, second, third and fourth derivatives and are typically approximated using Taylor series.

The conventional finite difference method utilizes a regular grid of nodes, such as a rectangular grid as shown in Figure 10. The grid system is a way of generating objective function values at sampling points with small enough intervals between them, so that introduced errors are small enough to be acceptable (Jing, 2003).

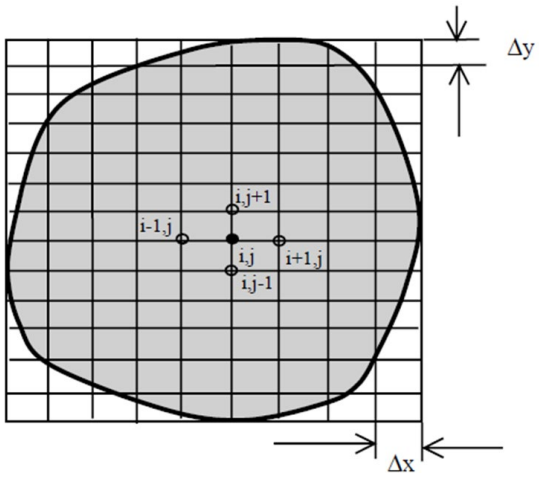

Figure 10 Regular quadrilateral grid for the FDM (after Wheel, 1995)

1.5.6.2 Finite Volume Method (FVM)

The finite volume method is also a direct approximation of partial differential equations, but in an integral sense. As a branch of FDM, the FVM can overcome the inflexibility of the grid generation and boundary conditions in the traditional FDM with unstructured grids of arbitrary shapes.

For both FDM and FVM no global system of equation in matrix form needs to be formed and solved. The solutions of the equations are localized, which is more efficient for memory and storage handling in computer implementation compared to a finite element method (FEM) problem.

Chapter 2 Methodology

The methodology is presented in two stages representing the two articles addressed in this thesis.

2.1 Adapting the B factor to account for major faults

Mathews' method for the calculation of the B factor using the orientation of major geological faults intersecting the different walls of each stope was used for the later calculation of the stability number.

As the procedure of calculating the B factor is straightforward once the relative orientation of the fault is defined, this section will focus on the method for the selection of faults in cases where multiple faults were present.

This study was developed with the kind collaboration of three mines from northern Chile which provided data of stopes (design and CMS) as well as geotechnical information about the rock mass, stress measurements, structural fabric and faults in the form of mapping charts for the various mine levels, and 3D CAD models. Using this information, a unified database of faults per stope was made.

Table 2 presents the number of stopes used to generate both joint-based and fault-based databases for each one of the three mines. As the information is confidential, these three mines will be called Mine A, B and C. All mines had different sectors which will be numerically ordered.

Table 2 Number of stopes used to generate the databases

Mine	*Sector*	*Stopes*
A	*1*	*28*
	2	*11*
	3	*29*
	4	*20*
	5	*18*
B	*1*	*30*
	2	*14*
	3	*27*
	4	*8*
	5	*1*
C	*1*	*4*
	2	*9*
	3	*19*
	4	*40*
Total		***258***

As the faults' orientation is the most important feature to be considered for the calculation of the B factor, their strike and dip had to be measured for each one of the faults

intersecting stopes. This was done in most cases using the 3D CAD models and directly measured.

In case of multiple faults intersecting a stope face, the most critical structure was chosen for the calculation of the B factor. The criterion for choosing the most critical fault is similar to the one presented in (1.5.2) in which the user must consider the potential effects of each fault in the stability of the stope face. Relevant aspects include the fault's orientation relative to the stope face, its point (line) of intersection with the wall, its thickness and, if available, the strength of its filling.

An example of this is presented by Figure 11 where multiple faults intersect a stope. In this example, the fault marked in red was chosen for the stope's back wall as it is the most critical based on the B charts.

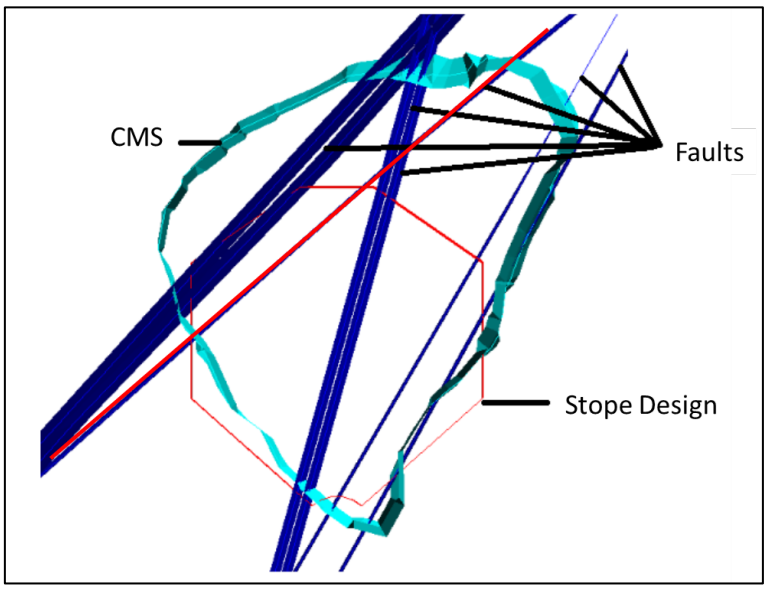

Figure 11 Example of stope being intersected by multiple faults.

Once the B factors for each stope face was obtained and the stability number N was calculated, a stability boundary was adjusted seeking to maximize the PSS (1.5.5.3). A higher PSS implies a better representation of stable and unstable cases.

With the stability boundary adjusted using the B factor from faults, and the stability boundary adjusted using the joints, an assessment of the reliability of the boundary can be done by comparing the PSS obtained with each boundary.

2.2 Obtaining an F factor

2.2.1 F factor calculation

The F factor of a stope back is obtained by comparing the overbreak volume produced in a stope that is intercepted by a fault, against a stope that is not. As this is empirically impractical, numerical modeling must be used. Numerical modelling allows for the

interpretation of multiple stope-fault interaction scenarios. A base case with no fault is used as a mean of isolating the overbreak attributed specifically to the fault in the other cases. Once the overbreak volume is measured for the base case and for a fault case, the F factor can be calculated using two different methods.

The first method is by direct comparison of overbreak volume of the two cases. The F factor is calculated as a fraction of the overbreak volumes as shown in equation (10). This method is simple, and no previous database is needed.

$$F = \frac{V_0}{V_F} \tag{10}$$

Where V_0 is the overbreak volume of the base case (with no fault) and V_F is the overbreak volume of the fault case.

The second method was originally introduced by Suorineni (1998) as a comparison of stability number N. For this method to be used, a dilution-based stability graph such as the one introduced by Clark & Pakalnis (1997) must be used. It is preferable to use a graph generated with local performance data, so that the estimated F factor better represents the influence of local faults as opposed to the results obtained using an externally generated stability graph.

The calculation of the F factor using the Suorineni (1998) method is done in four steps:

1. From the results of numerical models, the overbreak volume of base case and fault cases must be precisely measured.

2. Knowing the overbreak volume and the designed dimensions of the stope back, the Equivalent Linear Overbreak/Slough (ELOS) must be calculated for each case using equation (4).

3. Using an ELOS based stability graph, one must enter the chart from the hydraulic radius axis of each case. A vertical line is traced from each case's hydraulic radius to the ELOS curve representing the ELOS calculated in step 2. From the point of interception, a horizontal line is traced to determine the corresponding stability number. This is done for both the base case and the fault case, obtaining two N values as a result.

4. The F factor is finally calculated as a fraction of the N values obtained in step 3 as shown in equation (11).

$$F = \frac{N_F}{N_0} \tag{11}$$

Where N_F and N_0 are the stability number for the fault case and the base case, respectively.

An advantage of this method is that it takes into account the exponential nature of the stability number N, whereas the first method directly compares the overbreak volumes.

The third step of the second method implies the interception of an ELOS stability curve of a certain value obtained in step 2. Since a discrete set of ELOS stability curves can be derived from any given database, an interpolation method must be used if the ELOS value calculated in step 2 does not match a specific ELOS curve.

The interpolation method used in this study is shown in equation (12):

$$N = a \cdot ELOS^{-c} \cdot HR^{b} \tag{12}$$

Where constants a, b and c must be adjusted to fit the interpolated curves to empirically generated ones.

The method allows the possibility of estimating the stability number N of a numerically modeled stope face based on its resulting overbreak volume or ELOS and its hydraulic radius.

The stability boundaries used for the calculation of constants a, b and c used in this study were generated from an empirical database built for the same underground mine as the stopes used in the calibration of the numerical models. These stability boundaries and further information about their adjustment can be found in Azorin (2019).

2.2.2 Numerical modelling

2.2.2.1 Calibration models

For the F factor to better represent the influence of local faults on stope stability, the numerical models must be calibrated to represent the performance of existing stopes. This was achieved selecting several existing stopes where the overbreak and the final shape of the walls was clearly affected by the presence of faults like the example shown in Figure 12. Once the stopes with faults were selected, a base case with no fault is also selected for reference. For each selected stope, a numerical model is constructed using the stope's original design.

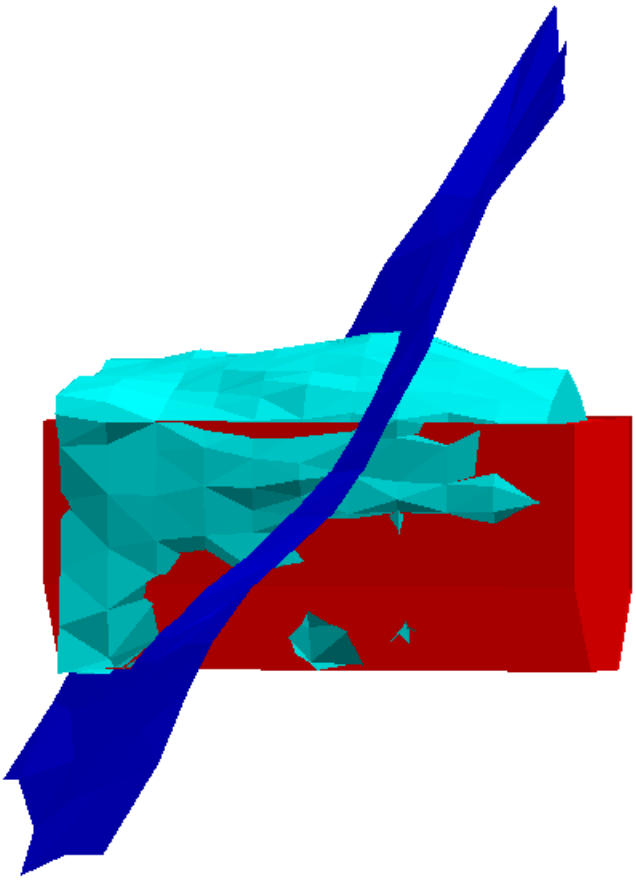

Figure 12 Example of stope's overbreak being affected by a fault.

Measurements of in-situ stresses are used as inputs and elasto-plastic constitutive models are used to represent the mechanic behavior of the rock mass and fault. While a Mohr-Coulomb linear failure envelope is used for the faults, a generalized Hoek-Brown nonlinear envelope is used for the rock mass.

Plasticity state will be represented by Hoek-Brown's failure envelope. This non-linear criterion relates major and minor principal stresses according to the equation shown in Figure 13.

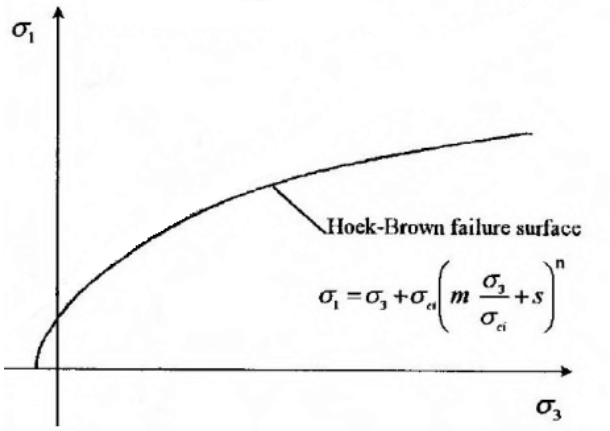

Figure 13 Hoek-Brown failure criterion. Modified from W. Wu (2015)

where σ_{ci} is the unconfined compressive strength of the intact rock, and m, s and n are material constants that can be related to the geological strength index and rock damage (Hoek et al. 2002).
If at some point of the modelling instance of the stope, fault and rock mass, if any element of the mesh is exposed to principal stresses plotting over the strength envelope, the element will yield and become acquire a plastic state.

The numerical model runs in three steps: elastic pre-excavation, elasto-plastic pre-excavation and elasto-plastic post excavation. Once the final equilibrium is reached, the volume of the yielded elements over the stope back is measured and the general shape of the overbreak region is visually assessed. The overbreak volume and the shape of the overbreak region of the modelled stopes are then compared with the ones obtained for the existing stopes using the C*avity Monitoring Survey* (CMS) 3D representation.

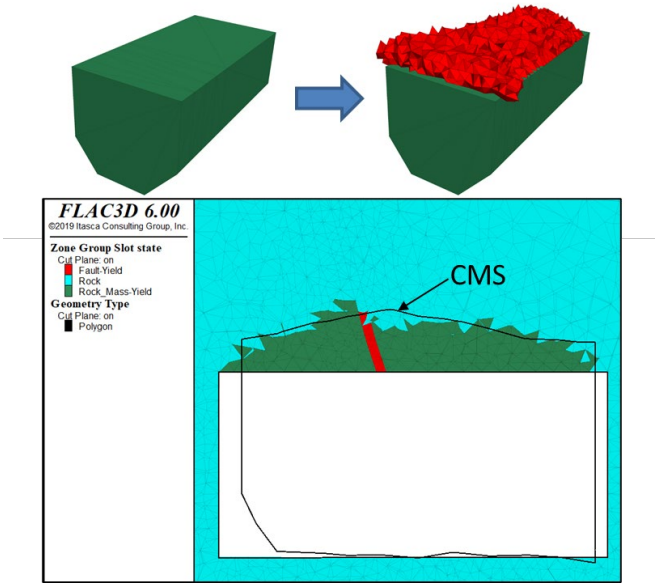

Figure 14 Upper portion: Representation of overbreak as yielded elements after model equilibrium. Lower portion: Comparison between modelled overbreak (green and red) vs reference CMS (black line).

The calibration process iterates changing fault strength properties and measuring the resulting overbreak volume. The difference between reference and modelled overbreak volume is then calculated and the difference percentage is obtained. The shape of the modelled overbreak volume is also visually compared to the CMS seeking a similar shape as shown in Figure 14.

2.2.2.2 Synthetic models

Once the strength parameters are calibrated (Table 4 and Table 5), the synthetic models can be constructed. The stope used for all the synthetic models is box shaped and is placed the center of a cubic box of 400 m side to avoid boundary effects. The stope's dimensions are presented in Table 3 The fault's thickness is six meters, and its orientation is variable. An example of mesh for synthetic model is shown in Figure 15. The stope is in the center of the box.

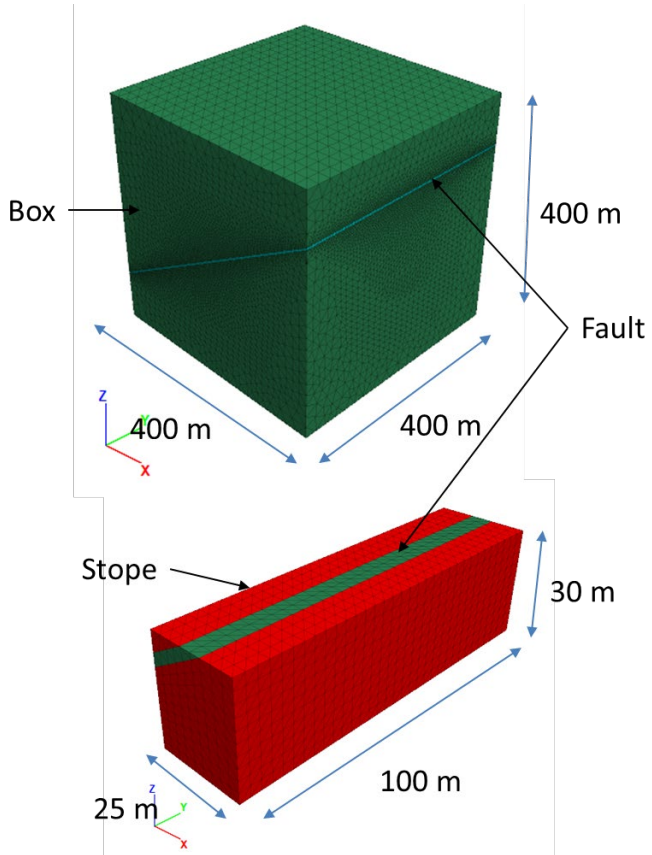

Figure 15 Upper portion: Box mesh. Lower portion: Stope mesh.

Table 3 Dimensions of stope used iin synthetic models.

Dimensions	*Unit*	*Value*
Length	*m*	*100*
Width	*m*	*25*
Heigh	*m*	*30*

While the stope is aligned with the N-S axis for all synthetic models, three strikes were used for the fault (0°, 45° and 90°). This means the fault is either parallel, diagonal or perpendicular to the stope. The fault's dip is also variable, and for each different strike configuration, three dips were assessed: 90°, 60° and 30°. In addition to these nine combinations, other models were constructed with a horizontal fault (0° dip). These models place the fault at different distances from the stope back to assess the influence of vertical distance from the back on the stability and overbreak volume.

Table 4 Strength parameters for the rock mass used in synthetic models.

Property	*Unit*	*Value*
Density	*kg/m3*	*2600*
σ_{ci}	*MPa*	*200 - 250*
GSI	*#*	*50 - 60*
m_i	*#*	*15 - 20*
D	*#*	*0.3 - 0.5*

E_i	GPa	60 - 80

Table 5 Strength parameters for the fault used in synthetic models.

Property	Unit	Value
Density	kg/m3	2100
Cohesion	KPa	10 - 20
Friction Angle	(°)	20 - 25
E_{rm}	MPa	200 - 500

In the cases where the fault is parallel to the stope, two intersecting positions were modeled. First, three models (representing the three dip values) intersect along the middle of the stope back and second, three models have the intersection at the stope back far edge (see Figure 15).

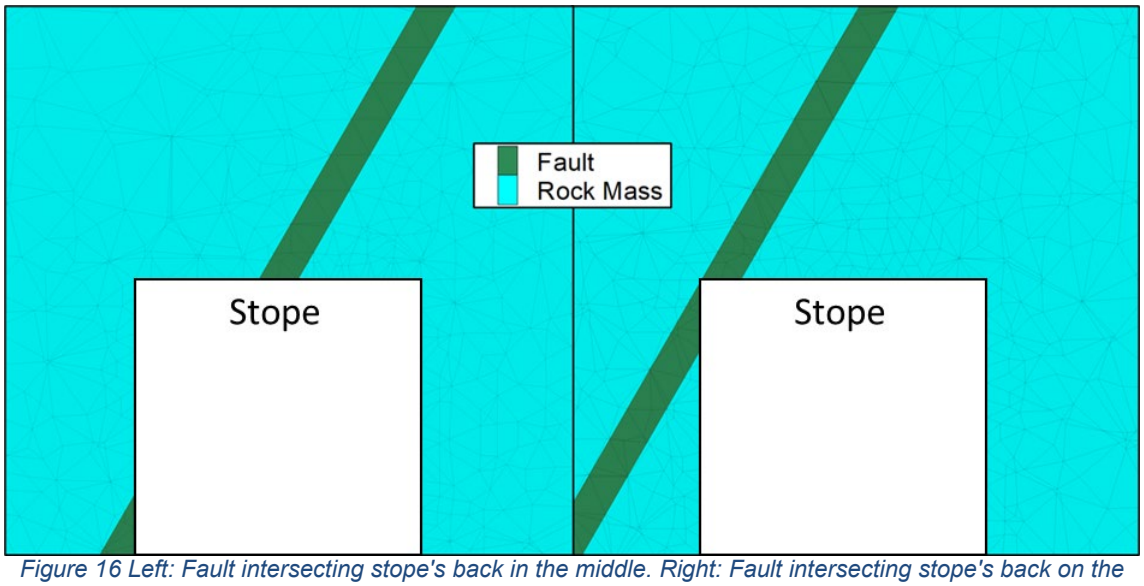

Figure 16 Left: Fault intersecting stope's back in the middle. Right: Fault intersecting stope's back on the side.

Finally, a model with no fault was made to use as reference. In total, 17 synthetic models were evaluated. As in the calibration models, plasticity state was used as the overbreak criterion.

In order to reduce the effects of the in-situ stresses' orientation, a horizontal to vertical stress ratio of 1.6 was used for both horizontal directions (east-west and north-south). The stress values used for the synthetic models are shown in Table 6.

Table 6 In-situ stresses used in the synthetic models.

Direction	Unit	Value
xx	MPa	14
yy	MPa	14
zz	MPa	9

Each model was run in three stages, reaching mechanical equilibrium at the end of every stage. The first stage is elastic pre-mining and it starts after stress initialization. The

second stage is elasto-plastic pre-mining. Finally, the third stage is elasto-plastic post-mining. The excavation is done using FLAC3D "*relax excavate*" command which reduces the density and elastic modulus of a certain region over time until zero is reached. At this point the excavation is completed. This helps to limit rebound effects from unrealistic, instantaneous excavations.

Once mechanical equilibrium is reached, the volume of every yielded element located over the stope back is measured and the overbreak is calculated. Finally, with the overbreak volume of every case measured, the F factor is calculated using the two methods presented earlier.

Chapter 3 Results

3.1 Use of b factor from major geological faults' orientation on Mathews' stability graph method. A case study.

Two databases obtained from the same case studies have been compared. The first database was obtained calculating the stability number *N* using Mathews' original *B* factor accounting for joint influence on stope integrity, while the second was obtained by calculating the stability number using a *B* factor derived from the relative orientation of the stope faces to major faults. It must be noted that even for the second database, the same values of *B* as a function of β (angle between stope face and structure) were used and, in cases when no faults intersected the stope face, a *B* factor value of 1.0 was used.

As the joints emerge from the same geological phenomena that create major geological faults, these two types of structures often share the same orientation. This means that if a stope face is intersected by both joint and fault it is highly possible that the same β angle is formed. As stated previously, the same function of β is used to calculate *B* factor for faults which means a similar distribution of values is expected. Figure 16 presents the distribution of *B* factors values for joints (left) and faults (right).

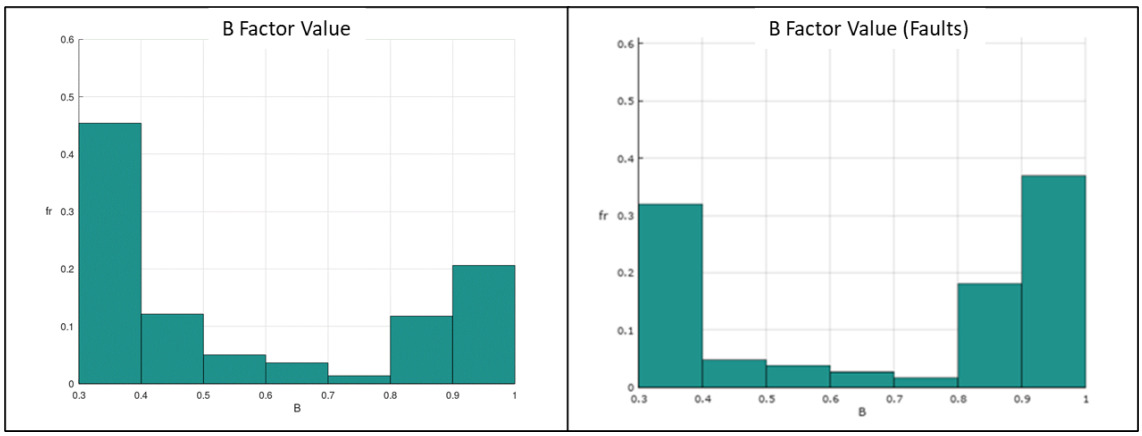

Figure 17 Distribution of B factor values for: (left) Mathews' original factor; (right) fault calculated factor.

3.1.1 Original Mathews' method

The graph in Figure 17 was obtained calculating stability number *N* using Mathews' *B* factor, which means the influence of joint orientation was considered. The stability curve which attains the best possible classification of stable/unstable cases reaches a PSS value of 0.36.

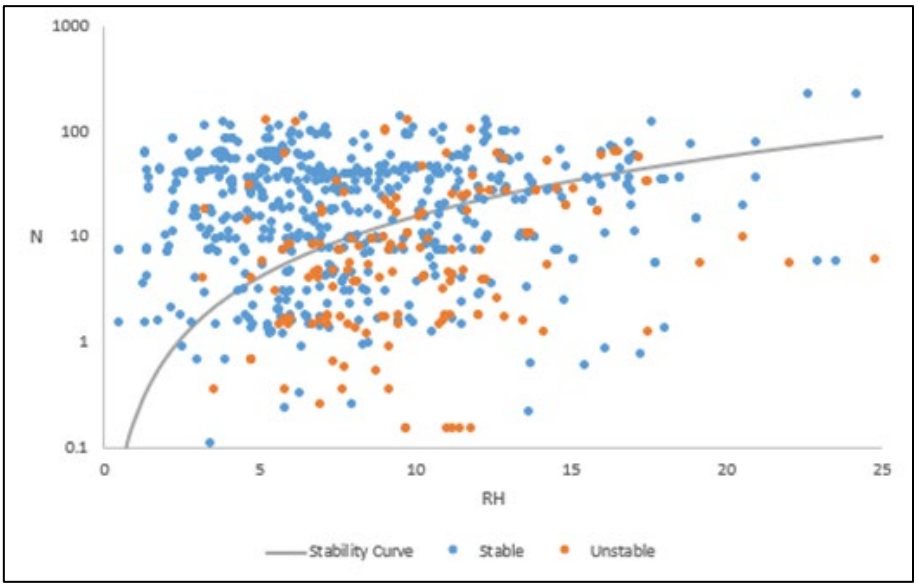

Figure 18 Stability graph. N calculated using Mathews' B factor.

3.1.2 Stability graph using B factor from faults

The graph in Figure 18 was obtained calculating stability number *N* using a *B* factor that accounts for the influence of major geological faults in the stability of the stopes' walls. The stability curve which attains the best possible classification of stable/unstable cases reaches a PSS value of 0.44.

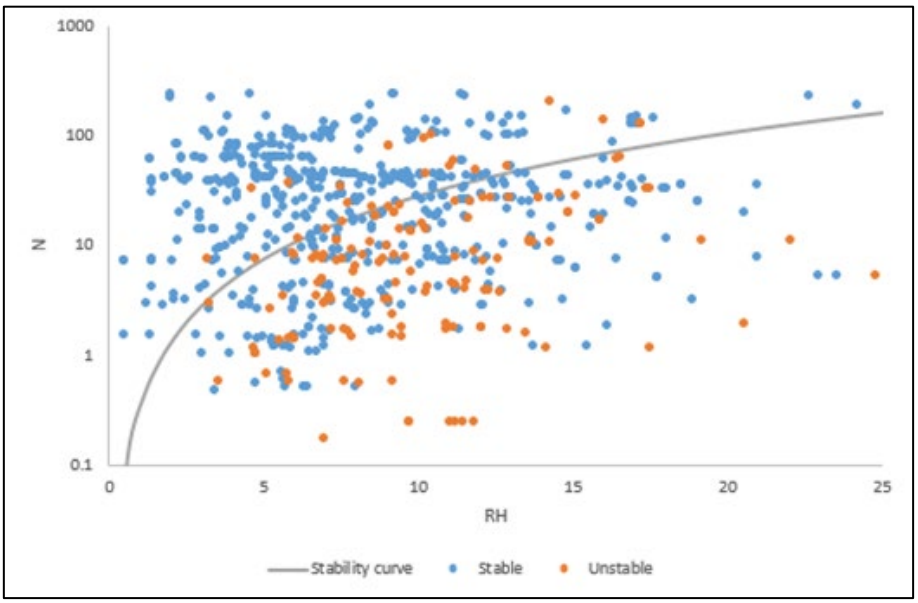

Figure 19 Stability graph. N calculated using B factor from faults.

3.1.3 Results comparison

Considering the large amount of cases included in the database, going from a PSS value of 0.36 to 0.44 is a considerable improvement.

A better PSS is obtained mostly because there are fewer false negative cases in the second graph meaning that fewer actual unstable cases are located above the stability boundary accounting for a lower *FPR* value as shown in Table 7.

These results are consistent with engineer's observation of the stopes' walls stability, as major geological faults have a bigger influence on stability of large stopes than joints and as it is less likely for a stope face to be intersected by a fault as is it is by a joint set.

Table 7 Results comparison for Mathews original B factor and B factor from major geological faults

	TPR	FPR	PSS
Mathews'	0.65	0.29	0.36
Faults'	0.57	0.14	0.44

3.2 F factor: Quantifying the impact of faults on open stope's back stability.

For the purpose of obtaining the overbreak volumes based on the elements' plasticity state, all different plasticity states were aggregated independent of their nature (ie. Shear, tension, shear-past, tension-past) as shown in Figure 19Figure 19. The different plasticity states can, however, give an idea of the causes of failure, and therefore help interpret the actual influence of the fault.

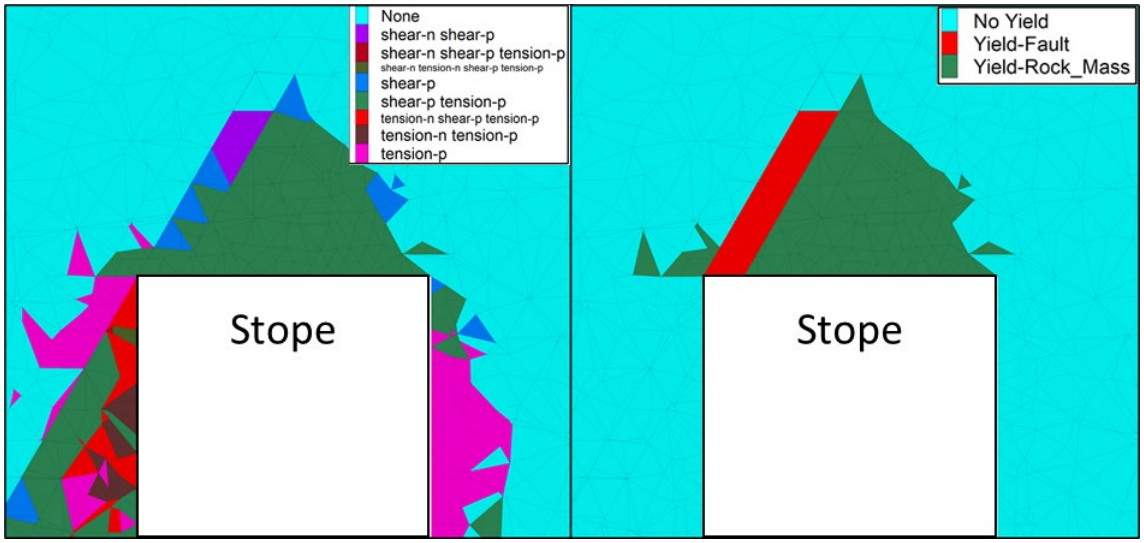

Figure 20 Left: Yielded elements separated by state. Right: Stope's back wall yielded elements grouped together.

The results from the different models were computed and plotted. In the cases where more than one case of a certain strike-dip configuration was run, such as dip 0, the case with the highest overbreak volume was considered.

3.2.1 F factor charts

The study presents two plots, one for each method introduced for the calculation of the F factor. Each plot has three curves, one for each fault's strike. The curves present the F factor as a function of the faults' dip. The plots are shown in Figure 20Figure 20 for method one and Figure 21 for method two.

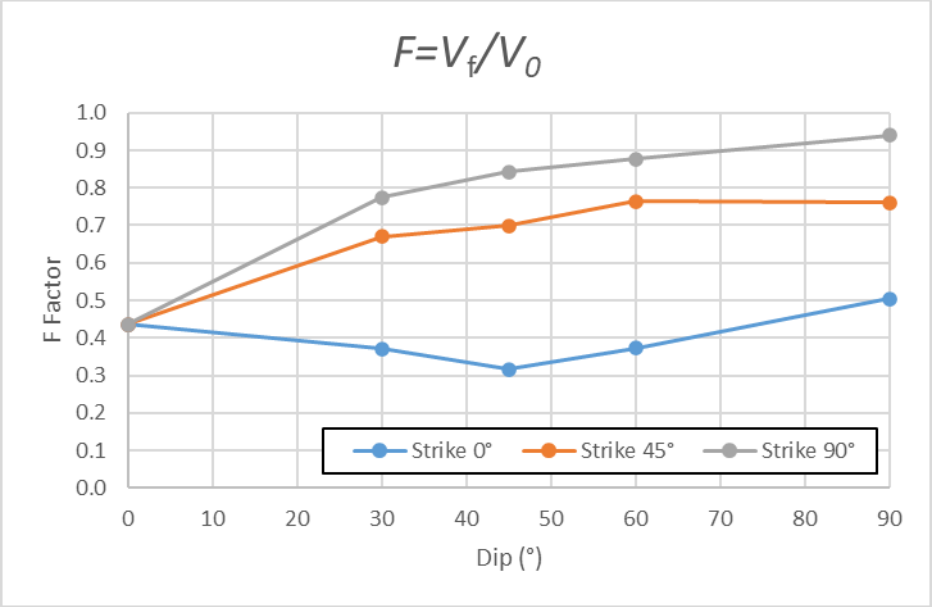

Figure 21 F Factor chart generated using method one.

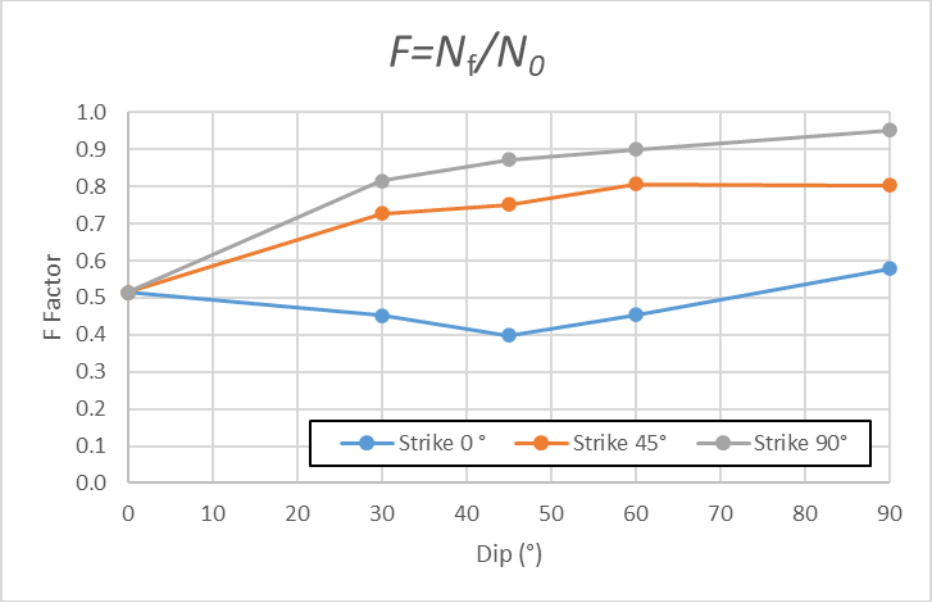

Figure 22 F Factor chart generated using method two.

Both plots present similar curves. Regarding the impact of fault strike, it can be seen that the worst case corresponds to a fault parallel to the stope, while a fault perpendicular to the stope proves to be the best scenario. The 45° strike case delivers less favorable results. The curves don't cross one another, and are more or less parallel.

For the two curves representing nonparallel faults, the 0° dip case is the least favorable. For both plots, all three curves start at the same point as the 0° dip case is the same for every strike. The different curves show that, as a rule, steeply dipping faults have less detrimental impact on stope back stability.

3.2.2 Effect of fault's distance to the back

Five cases of 0° dip were modeled, placing the fault at different distances from the stope back. The results of these models show that there is a specific distance at which the horizontal fault's influence is maximized. Once this distance is surpassed, faults have diminishing effects on the stope's stability until, eventually, they have no influence at all. The plot of Figure 22 show the results of the different 0° dip models.

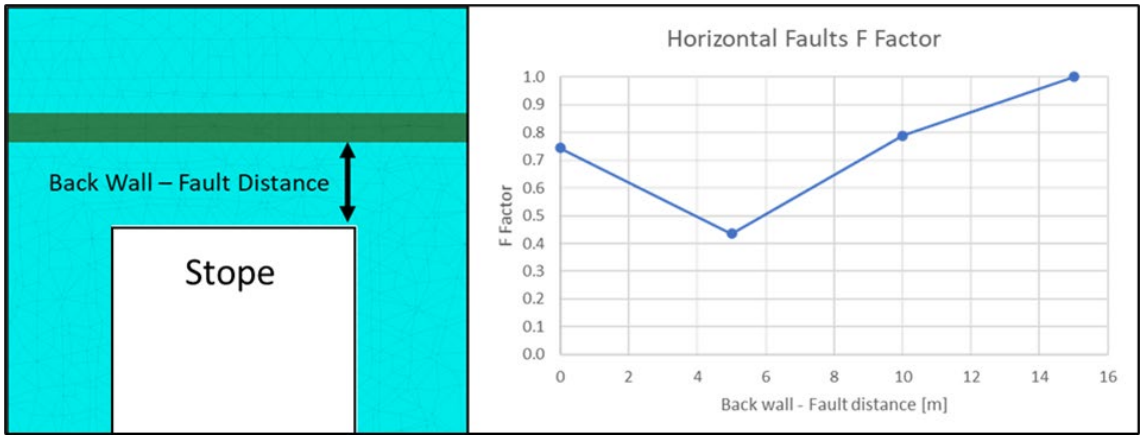

Figure 23 Results for horizontal faults. Method one.

3.2.3 Effect of fault's place of intersection

For the 0° strike cases, two models were made for each dip, locating the fault either at the edge or center of the stope back, as shown in Figure 15. The results of these models are shown in the plot presented in the chart of Figure 23 which has two curves, one for each position, and where both start at the same point as the 0° dip case is common to both.

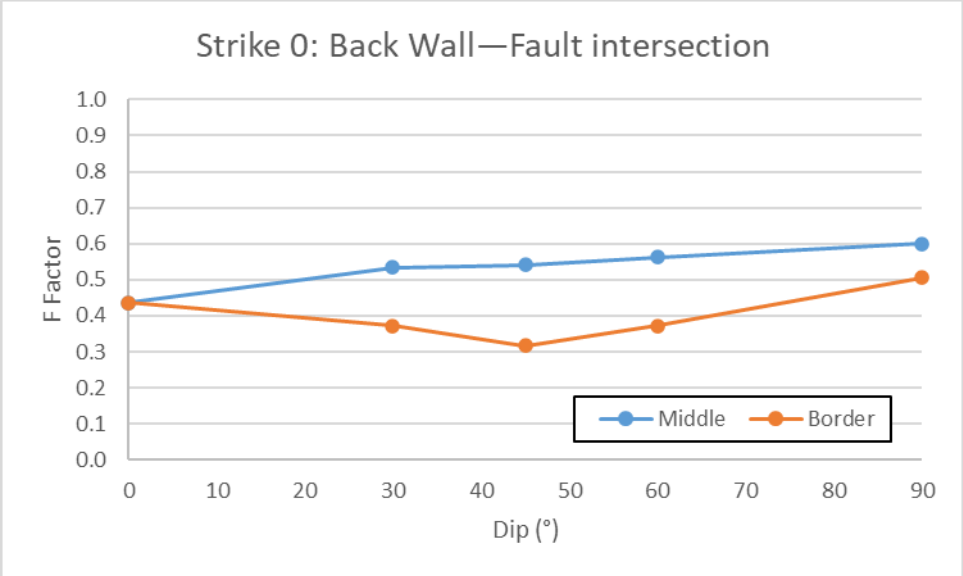

Figure 24 Results for Fault intersecting in the middle and side of the stope's back. Method one.

Regardless of the dip of the fault, an intersection at the stope back far edge bears greater impact than an intersection along the back's center axis. The difference is small for sub-horizontal faults and increases with fault dip until reaching a maximum at a dip of 45°, after which the effect again begins to decrease as the fault becomes steeper.

3.2.4 Results interpretation

The results used to generate the curves for the F factor only consider the overbreak volume to be the sum of yielded elements' volume regardless of their failure mechanism; however, the distribution of these mechanisms can help to understand the causes of the results shown in the plots and reveal the failure mechanism controlling the instability in each case as shown in Figure 19 (left).

The cases with sub-horizontal dipping faults show concentrations of tension-based plasticity over the stope back, which may be caused by the breaking of rock bridges extending form the wall to the fault. For sub-horizontal faults, the rock bridges are narrow and therefor easily broken by the stress relaxation created by the stope excavation. The numerical models are unable to represent the effects of blasting, but its effect on breaking rock bridges generated by joint sets is well known. This phenomenon likely occurs in the presence of faults as well.

For steeply dipping faults, the plasticity state dominating the overbreak volume is shear. The instability is controlled by blocks slipping along the fault and falling in the stope. Given the thickness of the rock bridges for these dip configurations, rock bridge breaking becomes increasingly more difficult and so overbreak volume decreases. Blasting can also promote the slabbing of blocks along the fault, increasing the dilution.

Vertical and sub-vertical dipping faults are the least detrimental to stope back stability. As no sub-parallel surface is formed relative to the stope back, the concept of broken rock bridges and slabbing does not apply. Slipping along the surface of the fault may still occur; however, in a region with horizontal major principal stress – which may be concentrated over the stope's back due to stress redistribution – slipping along the fault's surface becomes difficult. The main effect of the fault on the stope dilution is a consequence of the fault disturbing the stable arch of rock blocks formed after the excavation of the stope increasing its height and changing its regular shape.

Horizontal faults are approached differently in this study. Horizontal faults can easily disturb the stable rock arch which forms above the stope back. The distance between the planned back and the fault is of great relevance. The results shown in Figure 22 indicate that the overbreak volume is greatly affected by this distance.

The fault tends to redefine the stope back location, as its surface becomes the new excavation boundary. Starting exactly at the stope back and increasing the distance, the more distance there is between the fault and the stope back, the more overbreak volume is generated. However, at a certain critical distance, the rock bridge is thick enough to resist under the resulting stress state. At this point, the fault no longer influences the stability of the stope back. This critical distance is logically influenced by other geotechnical parameters such as rock mass strength, in-situ stresses and blasting damage. Possible interactions between the stope back and subhorizontal faults beyond the back should be carefully approached in the design process.

The F factor plots presented in Figure 20 and Figure 21 consider the worst-case scenario for the 0° dip condition. However, to account for the variability introduced by the distance between fault and back wall, the segment between the first and second points of the plots (corresponding to faults parallel or subparallel to the back) may be replaced by a region as shown in Figure 24.

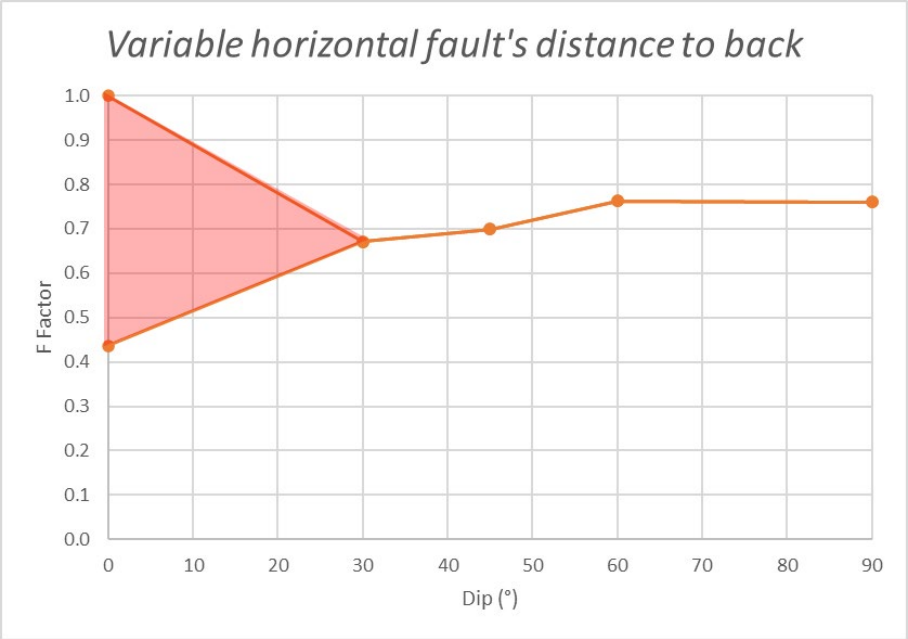

Figure 25 F Factor for the 45° strike case with variable horizontal fault's distance to the back wall. Method one.

The F factor curves show that for a scenario where a fault is parallel to the stope's strike, the fault's dip is of minor relevance. This is suggested by the minor variations of the F factor along this curve. This result may be influenced by the modeled stope dimensions, particularly, the back's shape factor. The place of intersection of the fault and the stope back is also relevant and can modify the general shape of the F factor curve. Even though only two points of intersection were modelled in this study, results show that if the distance between the line of intersection moves opposite to the fault dip direction, its impact decreases.

In this study, two scenarios were modelled for each 0° strike case and the worst result was always selected to construct the F factor curves. Even though this may not be representative of every possible outcome, it is considered a conservative approach and can be used if the construction of more representative F factor curves is not feasible.

Chapter 4 Conclusions and future works

4.1 Limitations of F factor

Interaction with multiple faults is common in a highly stressed setting such as near the convergence of tectonic plate boundaries. Stopes intersected by more than a single fault are not uncommon, and this presents a major limitation to the proposed F factor, which considers a single fault. As a general recommendation, in case of more than one fault intersecting a stope back, the most critically oriented structure should be used. This follows the same logical approach as the determination of Mathews' B factor for structural fabric. In the case of the F factor, the main concern when choosing the most critically oriented fault should always be its strike, as a fault that is parallel to the stope will have the greatest influence on stability.

The F factor plots presented in this study were generated using numerical models that assume rock mass strength parameters typically found in Chilean competent rock masses. Even though these plots can be used as a reference in the absence of benchmark data, they may not be representative of weaker rock mass environments.

4.2 Conclusions

The conclusions will be separated as to represent the main findings of each paper:

4.2.1 Conclusions of calculating B factor from faults' orientation

The stability graph constructed using *B* factor from major geological fault's orientation makes a better classification of stable/unstable stopes' walls than the one made using Mathews' original *B* factor. This is mainly explained by the fact that in large stopes, major geological faults have a greater influence on stope stability than minor structures such as joints. Furthermore:

- The new guidelines allow the design of optimized large stopes in terms of expected stability performance in major geological fault environment.
- New stability curves have been adjusted using local geological and operational information which means it should predict stopes' walls stability more accurately than Mathews' original stability graph when major faults intercept the stope.
- Largest over break volumes usually occur on the stope's back due to their size, vertical orientation and rock mass quality.
- The original B factor used in Mathews' stability graph does not necessarily reflect the failure mechanism produced by minor structures such as joints in large stopes in Chilean mines.
- There are structural features in major geological faults that are not considered for the calculation of this new B factor. Further research on the importance of

parameters such as a stope's shape factor, stope face dip, stress orientation, vertical to horizontal stress ratio, fault filling and thickness is advised in order to get a better grasp of fault influence on stope stability.

- Mathews' values for *B* factor were used in this analysis in order to compare the results against the original stability boundaries. Other values for *B* factor such as the ones from Potvin (1988) could also be assessed in future studies.

4.2.2 Conclusions of F factor

The F factor allows the quantification of the damage induced by the presence of a geological fault in the integrity of a stope back. The graphs presented in Figure 20 and Figure 21 can be used to obtain the F factor of a fault – stope interactions based on the fault strike and dip.

The charts generated using the two methods for the calculation of the F factor show that the volume comparison method proposed in this study yields practically the same results as the stability number comparison method. The advantages of the volume comparison method for F factor calculation are that it is simpler and faster to calculate and does not require an existing database.

A fault parallel to a stope is the worst-case scenario, as it has the greatest impact in the stope's back stability. On the other hand, a fault that is perpendicular to a stope presents the most favorable scenario. Intermediate scenarios (e.g., strike difference of 45°) yield intermediate results. If a fault's strike is parallel to a stope, its dip becomes less critical as, under this condition, the F factor values range from 0.4 to 0.6 regardless of the dip.

3D numerical model results can be used to interpret the failure mechanism at the stope back associated with the fault using yielded elements' state. A stope back's main source of damage associated with a sub-horizontal dipping fault is the breaking of rock bridges due to decompression and blasting, followed by the release of the resulting slabs. As the dip of the fault increases (ranging from 45° to 60°), the failure mechanism changes to sliding along the fault. Sub-vertical dipping faults don't generate rock bridges between them and the stope surface, so these do not produce overbreak in the same manner. Slip along sub-vertical faults is difficult as compressive stresses tend to prevent rock blocks from moving or falling.

The line where the fault intersects the stope back is relevant to the estimation of the impact the fault may have. Models with the fault intersecting at the edge of a stope back exhibited more overbreak volume than the models with the fault intersecting in the middle. Presumably, faults intersecting the stope back at a point closer to the "near" edge (opposite of the fault's dip direction) should have even milder influence on sloughing, although this needs verification. Sub-horizontal and sub-vertical faults had smaller difference in F factor value than medium dipping ones.

In the case of horizontal faults, there is a certain critical distance between fault and stope back that maximizes its influence on the stability. This distance is assumed to be dependent on rock mass strength and the stress distribution, among other parameters. In the case of the models constructed for this study, a distance of five meters resulted in the lowest F factor value. After surpassing this distance, the F factor improves until the fault has no appreciable effect on the stability of the stope.

The results for the horizontal faults suggest that the region of the F factor corresponding to subhorizontal faults (dip < 30°) may be interpreted as a band that narrows into a line as the dip increases, to account for the variable impact of fault's distance from the stope back.

4.2.3 Possible improvements and future works for the F factor

Future developments of the three-dimensional F factor shall include variability in the rock mass properties, with a similar approach to Suorineni's F factor.

The shape factor of the stope back used in this study played an important role on the general form of the F factor curves, particularly on the case of faults parallel to the stope. Presumably, a stope back with a shape factor close to 0.5 should produce F factor curves with similar values for the different strikes evaluated. The shape factor of the stope back should be included as an additional variable in future developments of the F factor.

The horizontal to vertical stress ratio used for the synthetic numerical models was the same for both cartesian axes (east-west and north-south). This was done to avoid any impacts of the stress orientation on the models results. However, the orientation of the principal stresses is known to influence the behavior of the rock mass near faults. In-situ stress orientation can either hinder or promote rock blocks sliding along a fault surface and, in doing so, influence dilution. Different ratios of horizontal stresses should be included on future developments of the F factor to quantify the influence of stress orientation.

The formation and development of a fault can often affect the surrounding rock mass. Be it through hydrothermal alteration, development of a shear zone or other geological phenomena, faults often weaken the rock mass around them. A weakened rock mass in the fault proximity was not considered in the development of the F factor, but it may be included in the future.

Rock mass reinforcements such as cable bolts can help maintain stope back stability for a given period. This mitigation is also applicable in the presence of faults. Numerical modelling codes such as Flac3D allow the inclusion of reinforcement, which could potentially alter the shape of the F factor's curves, especially in the lower dips portion of the chart where reinforcement may have a greater impact on stability and dilution.

Develop a new stability boundary using the same database used to generate the stability boundaries for the B factor using faults' orientation.

Chapter 5 Bibliography

1. *Barton, N., Lien, R., & Lunde, J. (1974). Engineer-ing classification of rock masses for the design of tunnel support. Rock Mechanics, 6(4), 189–236.*
2. *Bewick, R., & Kaiser, P. (2009, May). Numerical Assessment of Factor B in Mathews Method for Open Stope Design. In Proceedings of the 3rd CANUS Rock Mechanics Symposium, Toronto, ON, Canada (Vol. 1113).*
3. *Brady, B. H. G., & Brown, E. T. (2013). Rock me-chanics: for underground mining. Springer Sci-ence & Business Media.*
4. *Capes, G. W. (2009). Open stope hangingwall de-sign based on general and detailed data collection in unfavourable hangingwall conditions.*
5. *Clark, L., & Pakalnis, R. C. (1997). An empirical de-sign approach for estimating unplanned dilution from open stope hangingwalls and footwalls. In Proceedings of the 99th Annual General Meeting.*
6. *Giekie, S. A. (1880). On the Carboniferous Volcanic Rocks of the Basin of the Firth of Forth: Their Structure in the Field and Under the Microscope. Royal Society of Edinburgh.*
7. *Goodman, R. E., & Shi, G. (1985). Block theory and its application to rock engineering (Vol. 26). Pren-tice-Hall Englewood Cliffs, NJ.*
8. *Hadjigeorgiou, J., Leclair, J.G., and Potvin, Y. 1995. "An update of the stability graph method for open stope design." 97th CIM-AGM, Rock Mechanics and Strata Control Session. Halifax, Nova Scotia.*
9. *Hoek, E., Carranza-Torres, C., & Corkum, B. (2002). Hoek-Brown failure criterion-2002 edition. Proceedings of NARMS-Tac, 1(1), 267-273.*
10. *Itasca Consulting Group, Inc. (2019) FLAC3D — Fast Lagrangian Analysis of Continua in Three-Dimensions, Ver. 6.0. Minneapolis: Itasca.*
11. *Mathews, K. E., Hoek, E., Wyllie, D. C., & Stewart, S. B. V. (1980). Prediction of stable excavations for mining at depths below 1000 metres in hard rock. Canmet Report, 802–1571.*
12. *Mawdesley, C., Trueman, R., and Whiten, W.J. 2003. "Extending the Mathews stability graph for open-stope design." EBSCO Publishing.Miller, F., Potvin, Y., & Jacob, D. (1992). Laser measurement of open stope dilution. CIM(Canadian Mining and Metallurgical) Bulle-tin, 85(962), 96–102.*
13. *Nickson, S.D. 1992. Cable Support GUidelines for Underground Hard Rock Mine Operations. Master of Applied Science Thesis, Vancouver, British Columbia: University of British Columbia.*
14. *Norwegian Geotechnical Institute (NGI). 2015. "Using the Q-system - Rock Mass Classification and Support Design." Oslo, Norway.*
15. *Potvin, Y. (1988). Empirical open stope design in Canada. University of British Columbia.*

16. *Suorineni, F.T. (1998). Effects of faults and stress on open stope design. Ph.D. thesis, University of Waterloo, Waterloo, ON.*

17. *Stewart S. B. and Forsyth W. W., The Mathews method for open stope design. 1995, CIM bull, p. 45-53.*

18. *Trueman, R., Mikula, P., Mawdesley, C., Harries, N. 2000. "Experience in Australia with the application of the Mathews' method for open stope design." CIM Bulliten, 93. 162-167.*

19. *Vallejos, J. A., Miranda, O., Gary, C., & Delonca, A. (2015). Development of an integrated platform for stability analysis and design in sublevel stop-ing mines--MineRoc. Underground Design Methods 2015, 477–489.*

20. *Vallejos, J. A., Miranda, R., Burgos, L., Perez, E., & others. (2017). Development of New Design Tools for Open Stoping Underground Mines. In 51st US Rock Mechanics/Geomechanics Sympo-sium.*

21. *Vallejos, J. A., Miranda, O., Gary, C., & Delonca, A. (2015). Development of an integrated platform for stability analysis and design in sublevel stop-ing mines--MineRoc. Underground Design Methods 2015, 477–489.*

22. *Vallejos, J. A., Miranda, R., Burgos, L., Perez, E., & others. (2017). Development of New Design Tools for Open Stoping Underground Mines. In 51st US Rock Mechanics/Geomechanics Sympo-sium.*

23. *Wu, W. (2015). Analytical solutions to assess the stability of rock slopes subject to cracks via limit analysis. IOP Conference Series: Earth and Environmental Science. 26. 012057. 10.1088/1755-1315/26/1/012057.*

The papers presented in this thesis are the following:

- Use of b factor from major geological faults' orientation on mathews' stability graph method. a case study. (Presented in arma 2019)
- Quantifying the damage of faults on open-stope back wall stability using 3D elasto-plastic numerical modelling. (Sent to International Journal of Mining, Reclamation and Environment)

Annexed

In this appendix, section views of the results of the models used for the calculation of the F factor are presented.

Reference

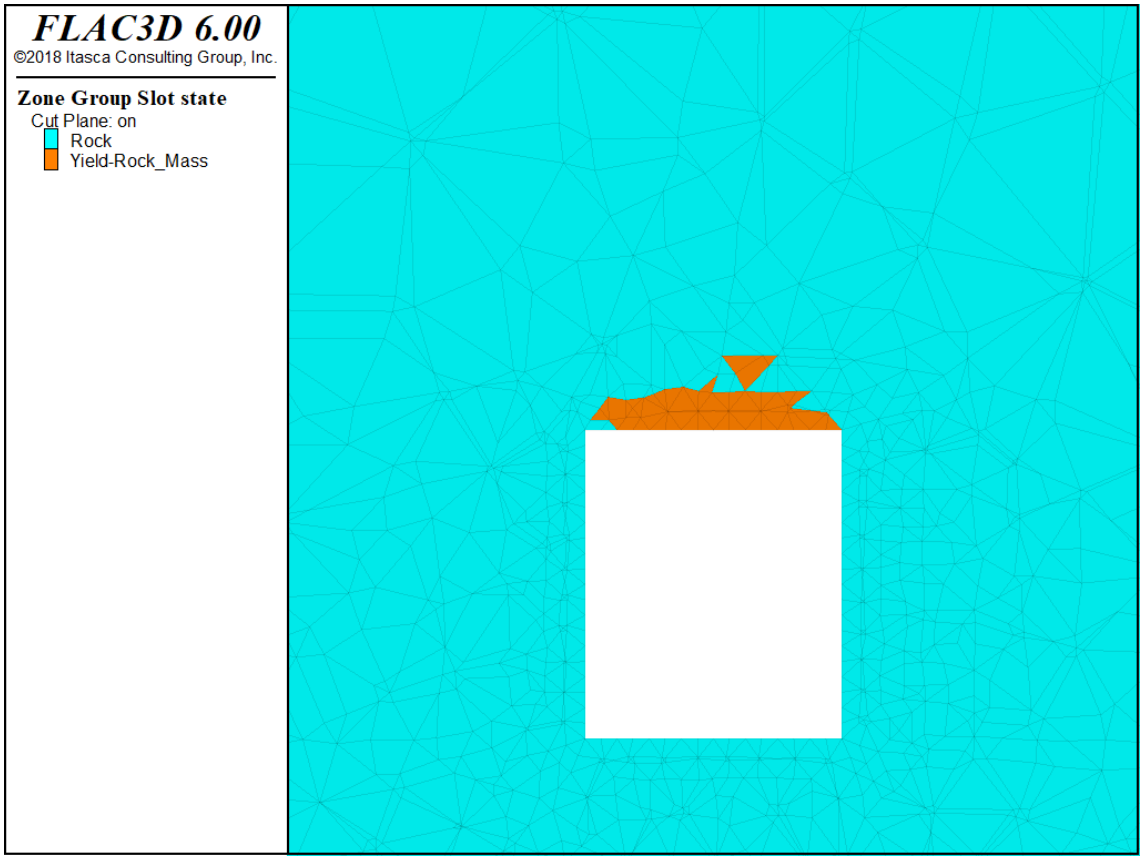

Figure 26 Reference case model

Strike 0°

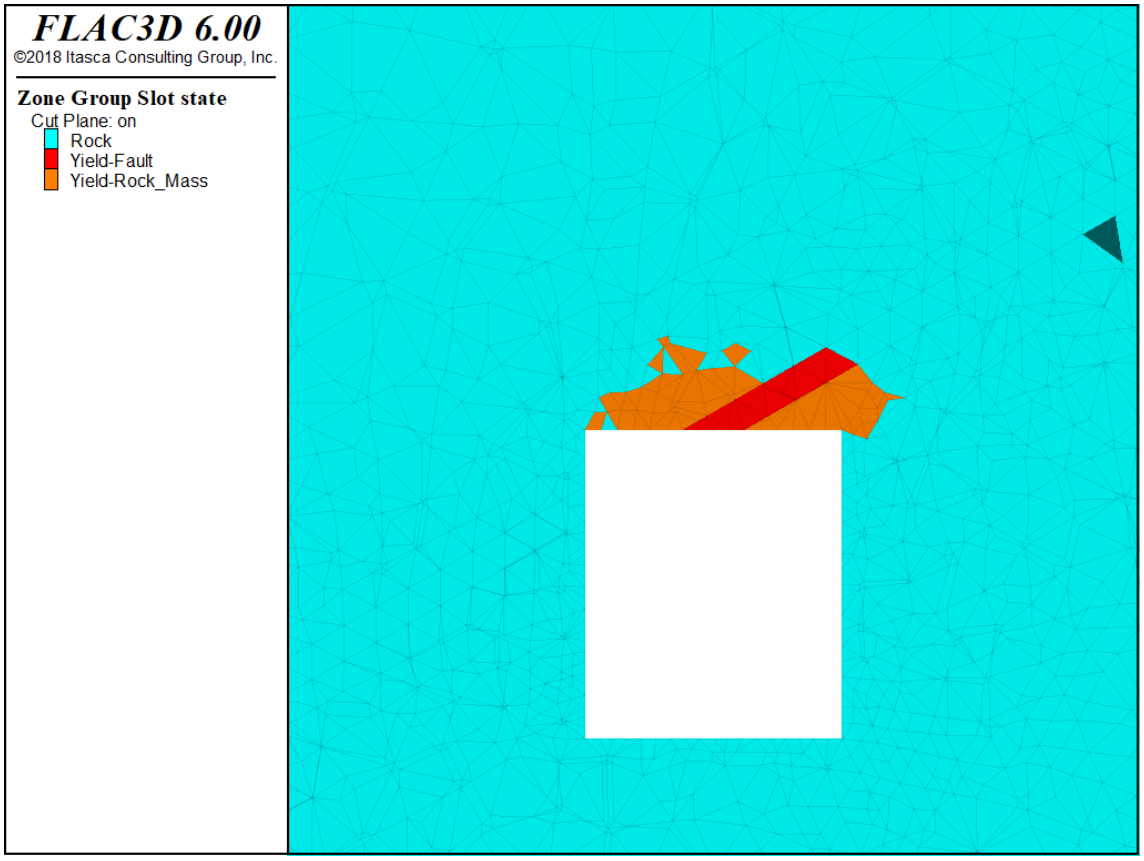

Figure 27 Strike 0, Dip 30, center intersection case model

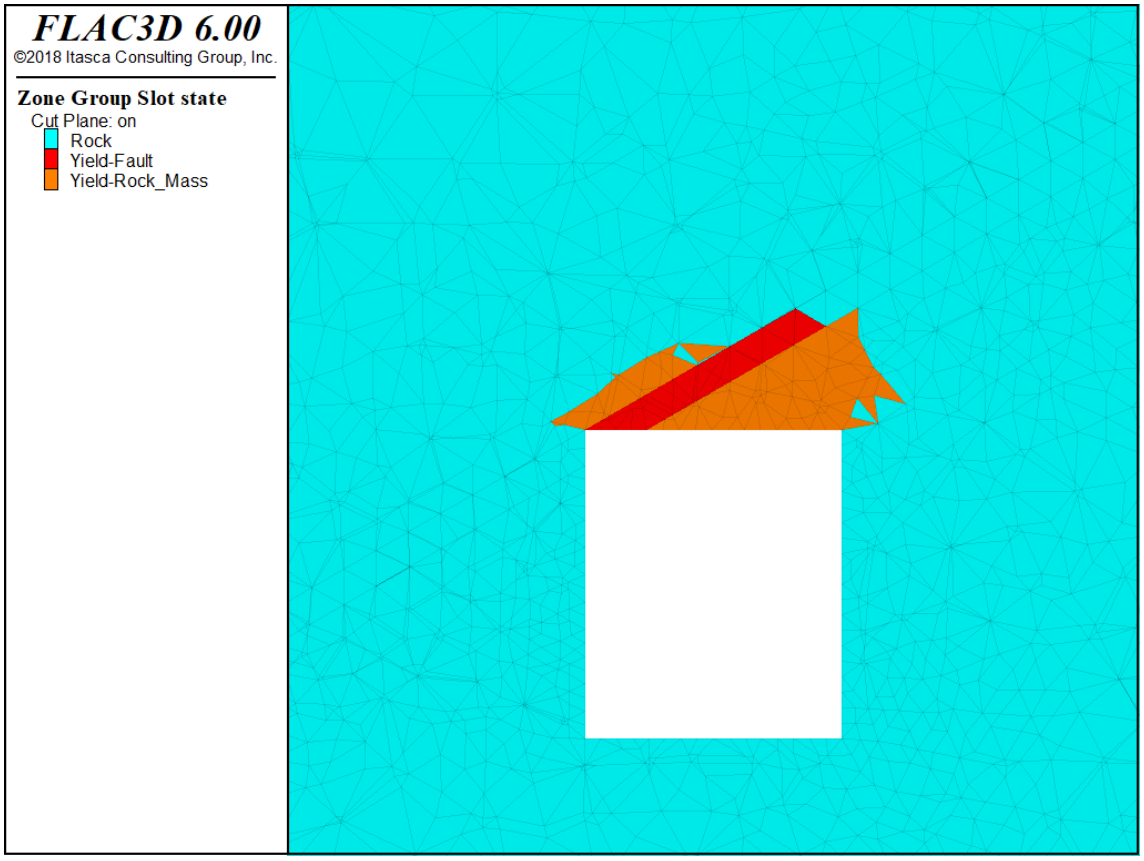

Figure 28 Strike 0, Dip 30, border intersection case model

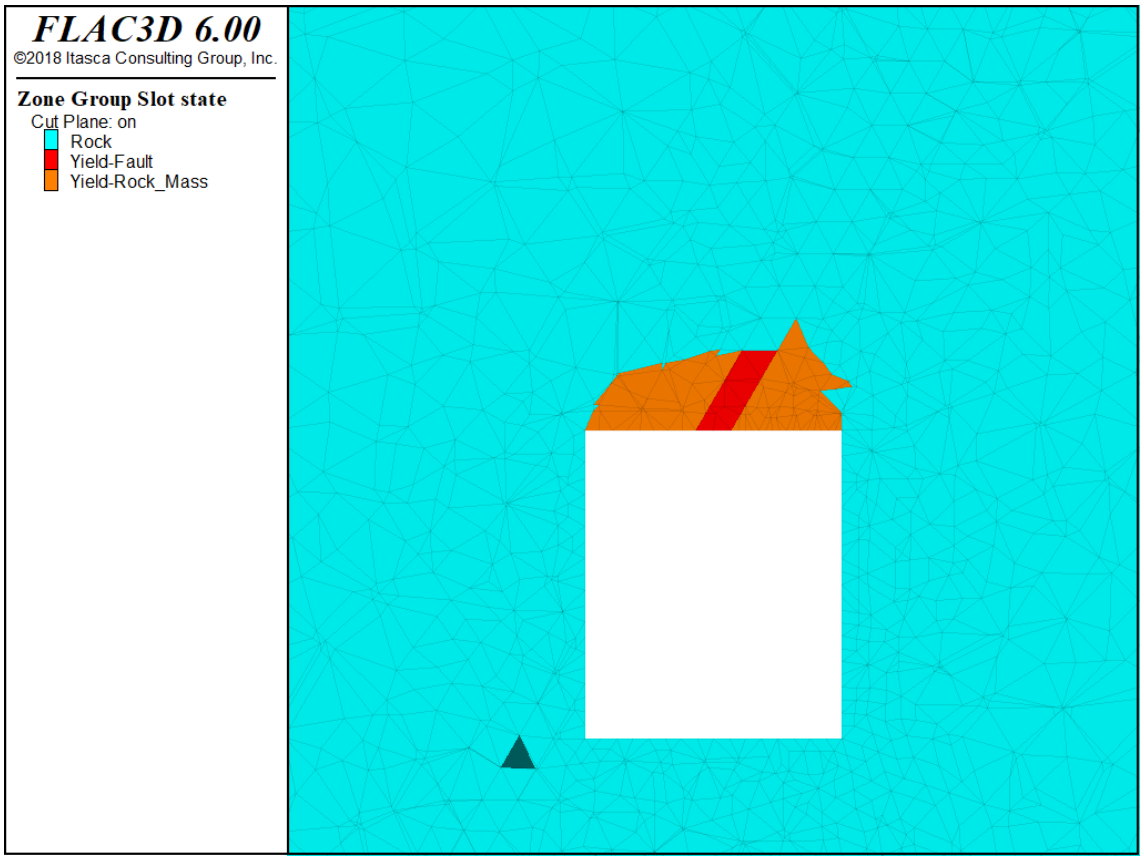

Figure 29 Strike 0, Dip 45, center intersection case model

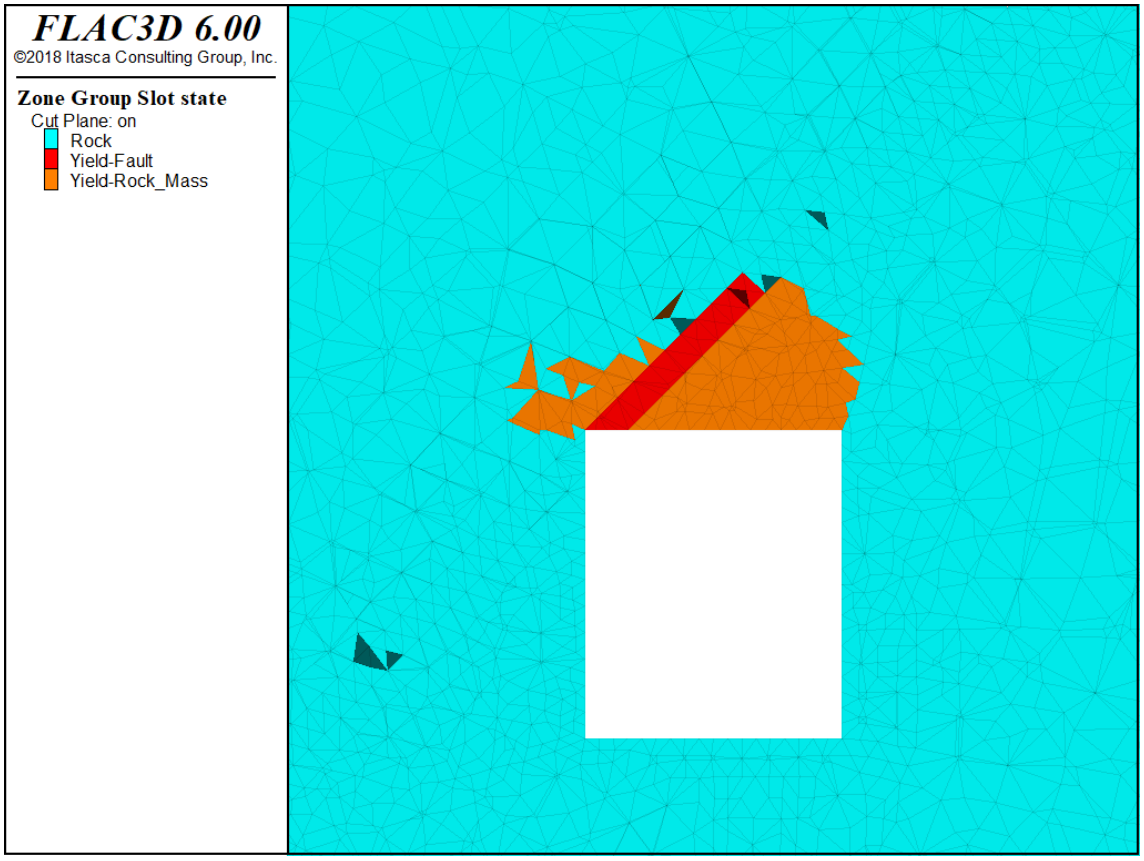

Figure 30 Strike 0, Dip 45, border intersection case model

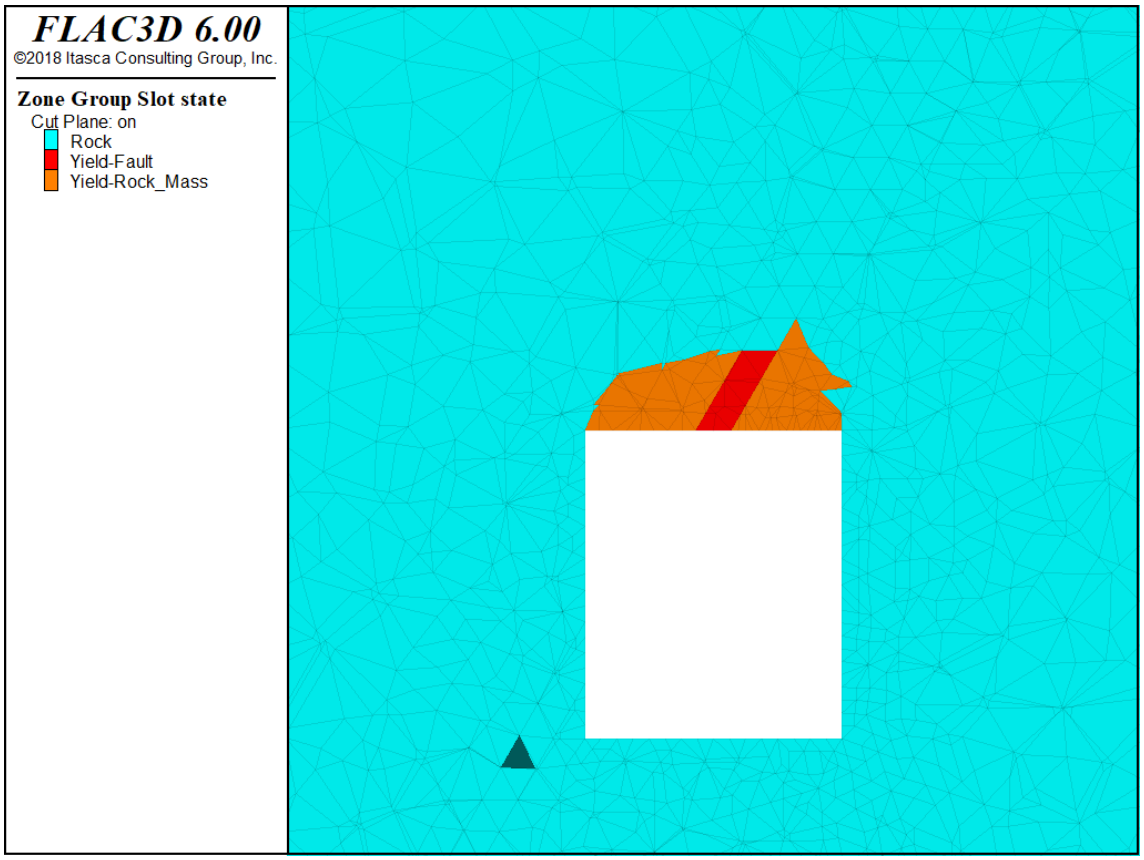

Figure 31 Strike 0, Dip 60, center intersection case model

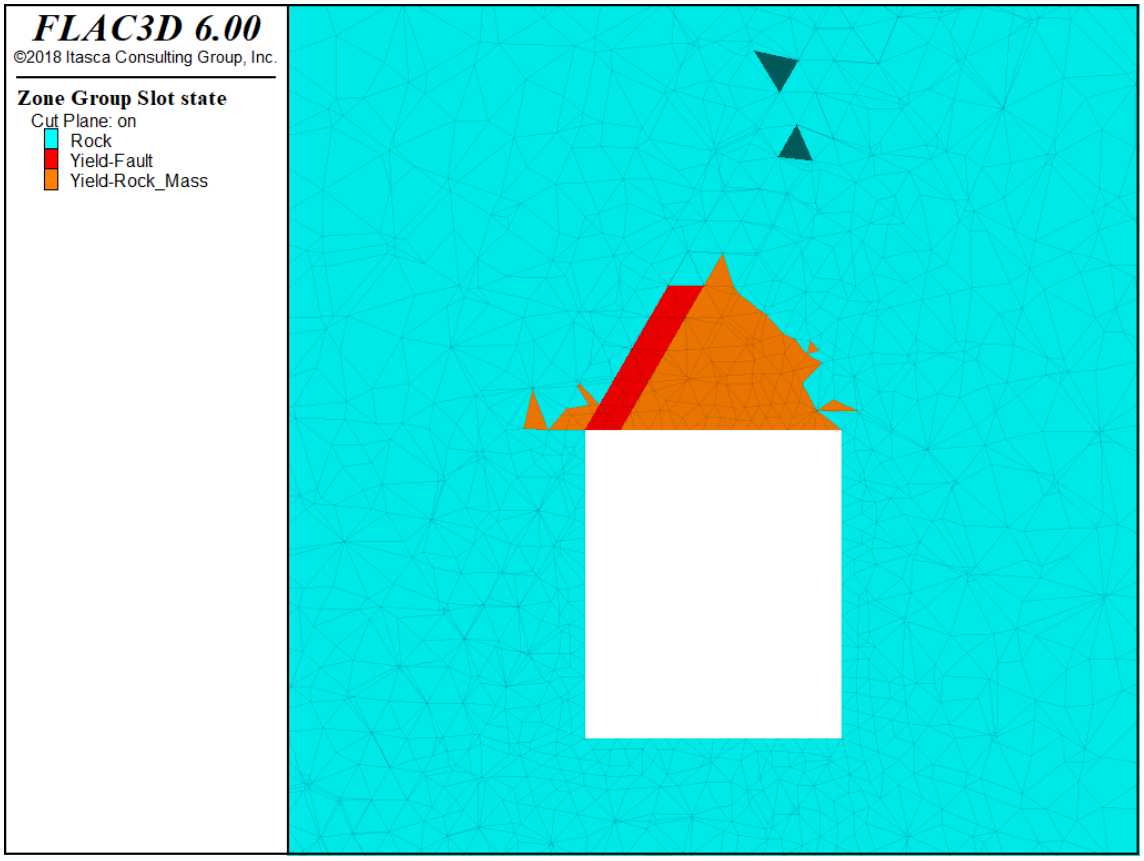

Figure 32 Strike 0, Dip 60, border intersection case model

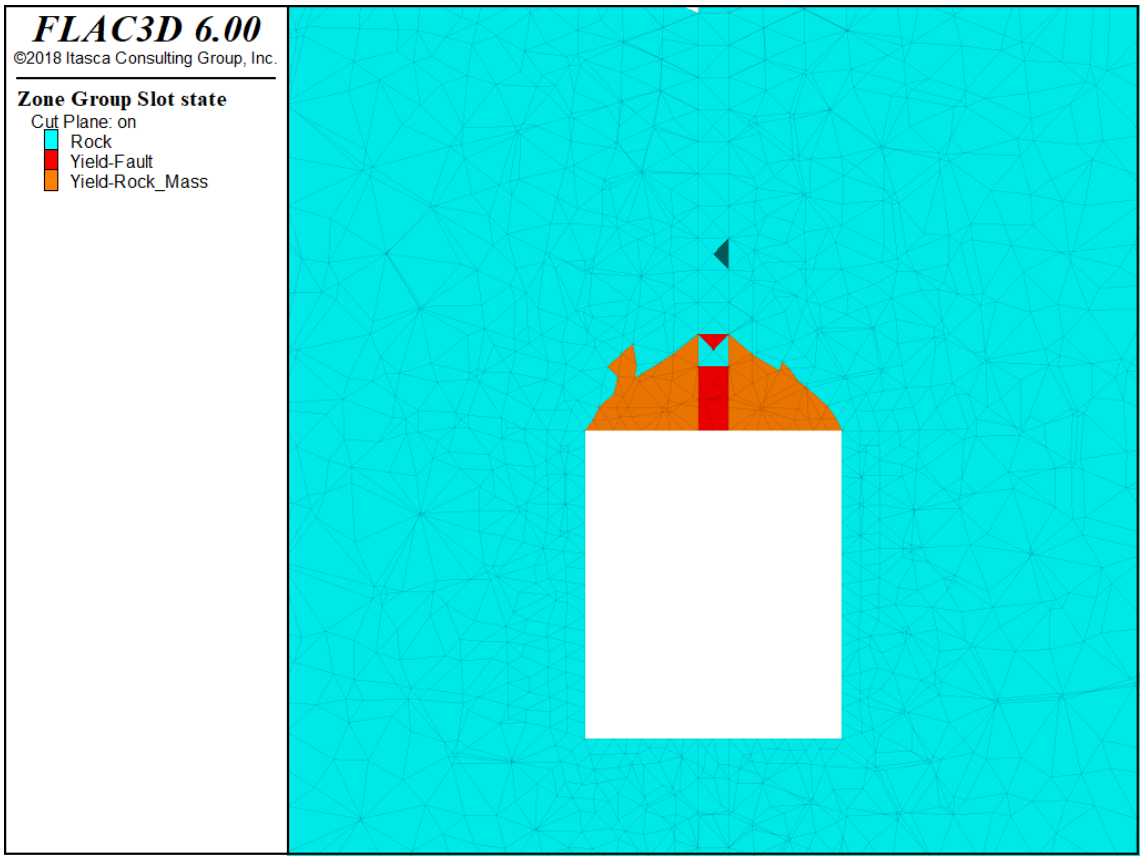

Figure 33 Strike 0, Dip 90, center intersection case model

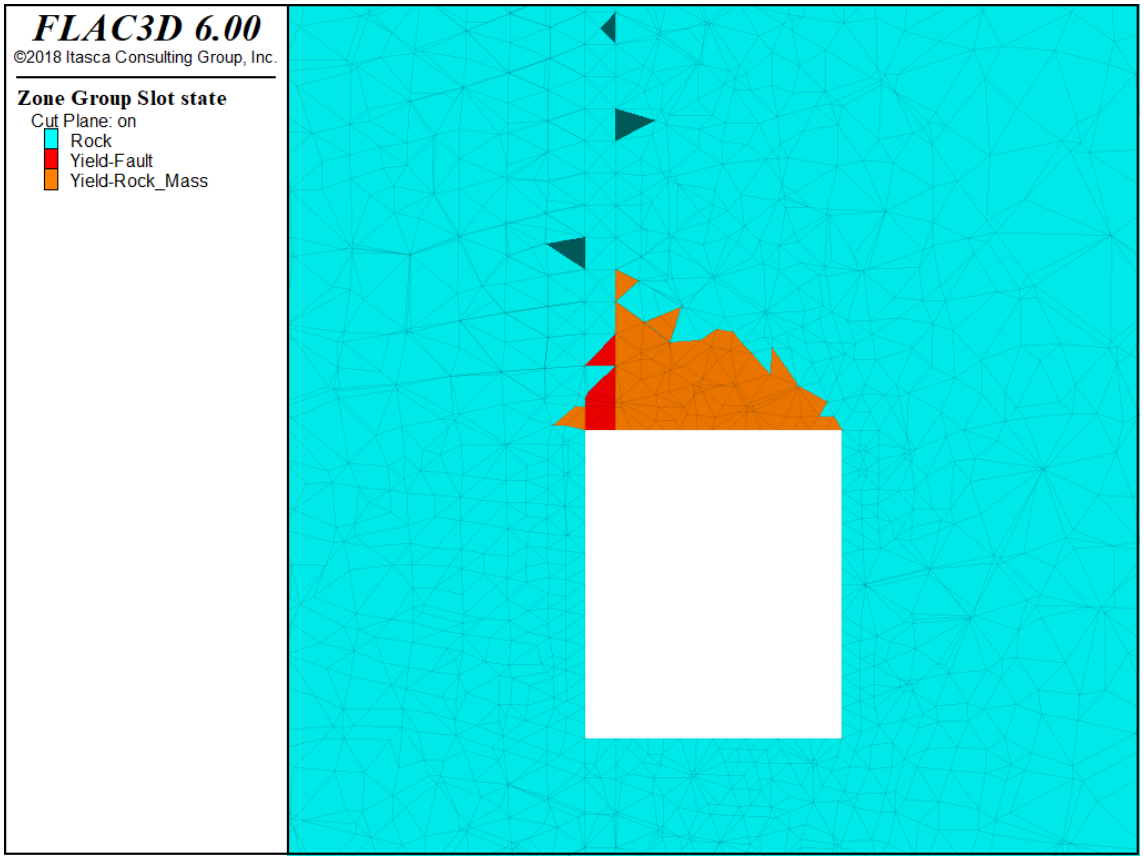

Figure 34 Strike 0, Dip 90, border intersection case model

Strike 45°

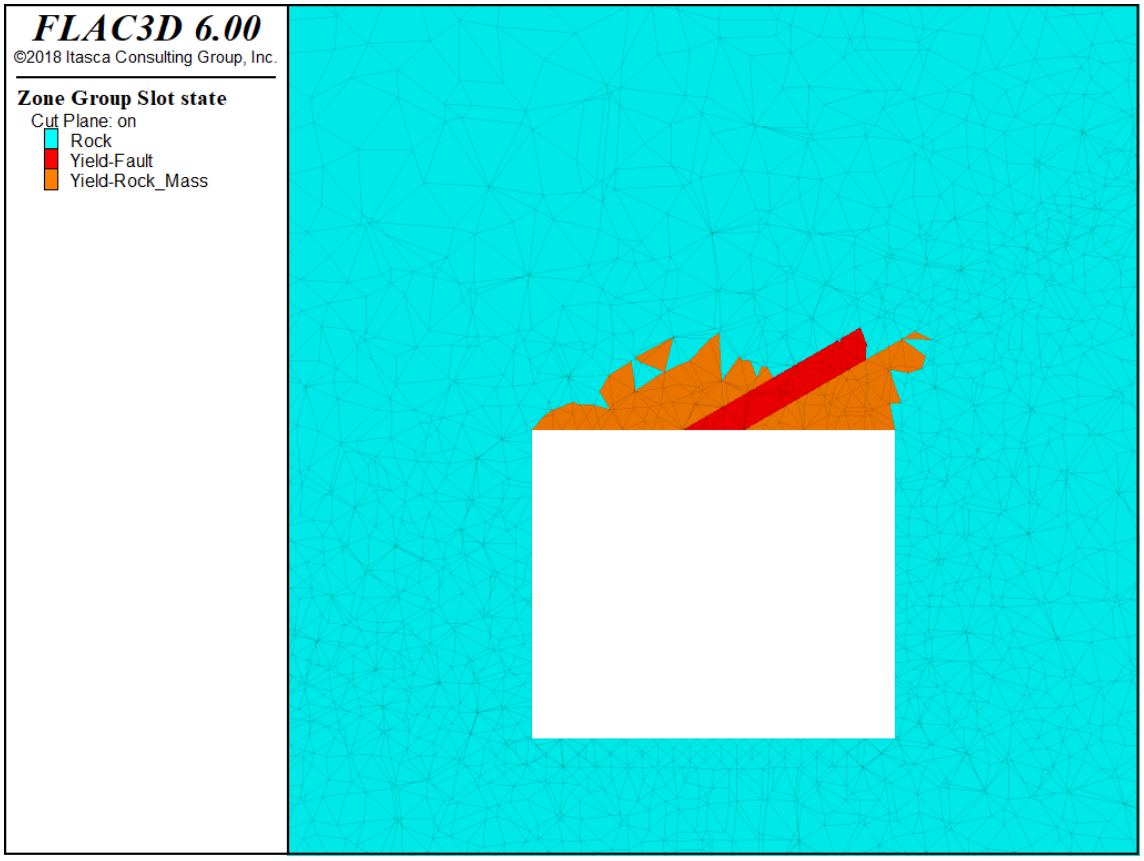

Figure 35 Strike 45, Dip 30 case model

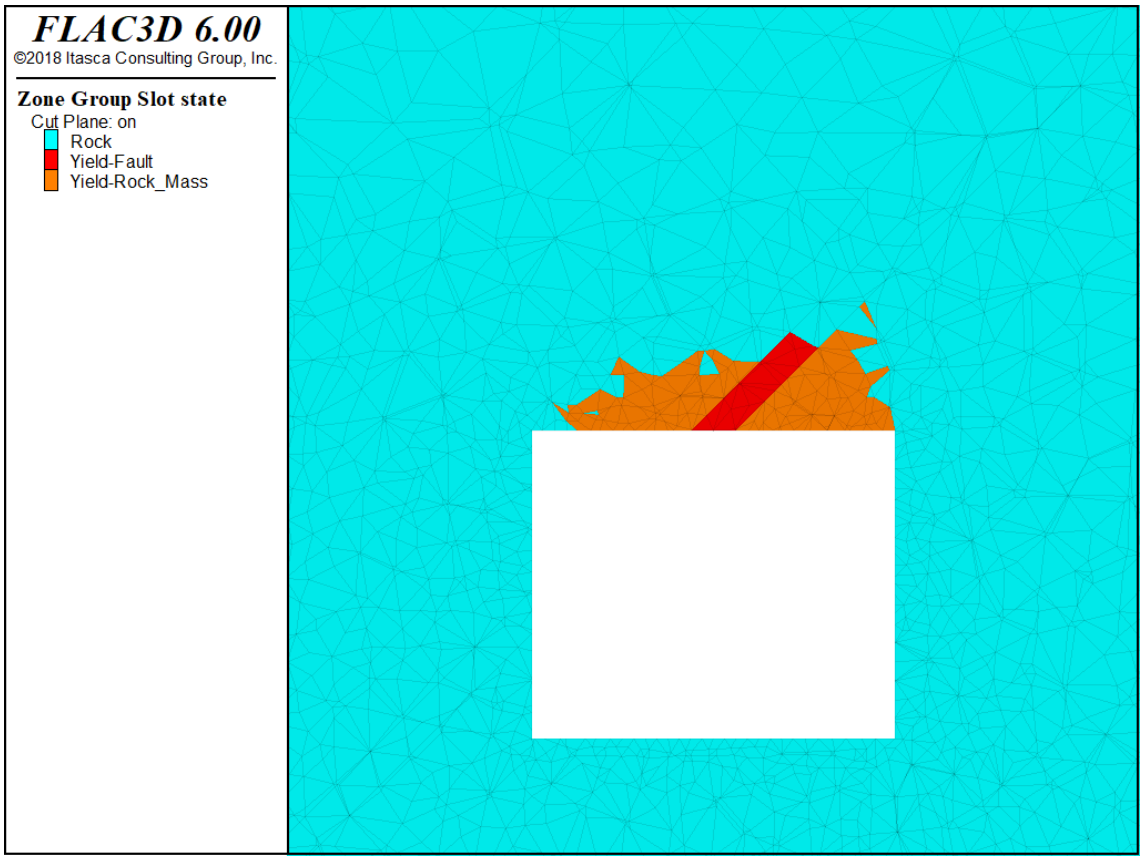

Figure 36 Strike 45, Dip 45 case model

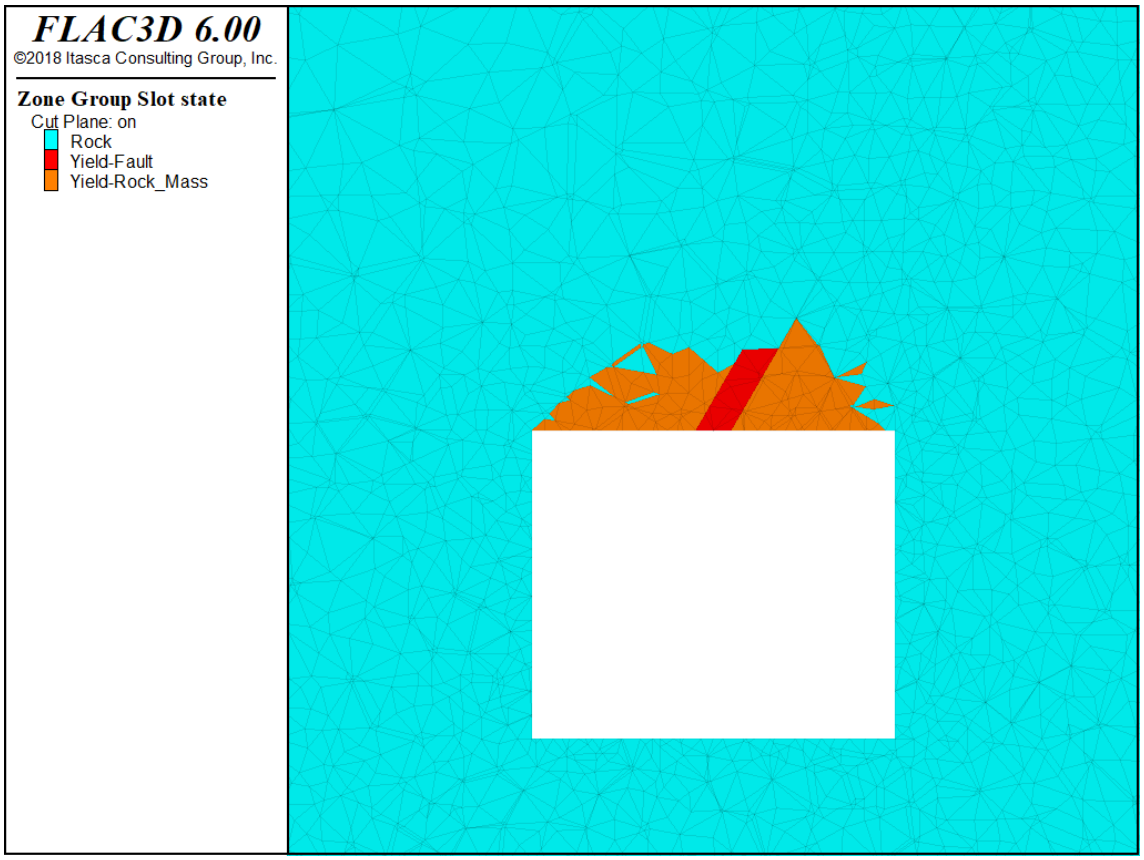

Figure 37 Strike 45, Dip 60 case model

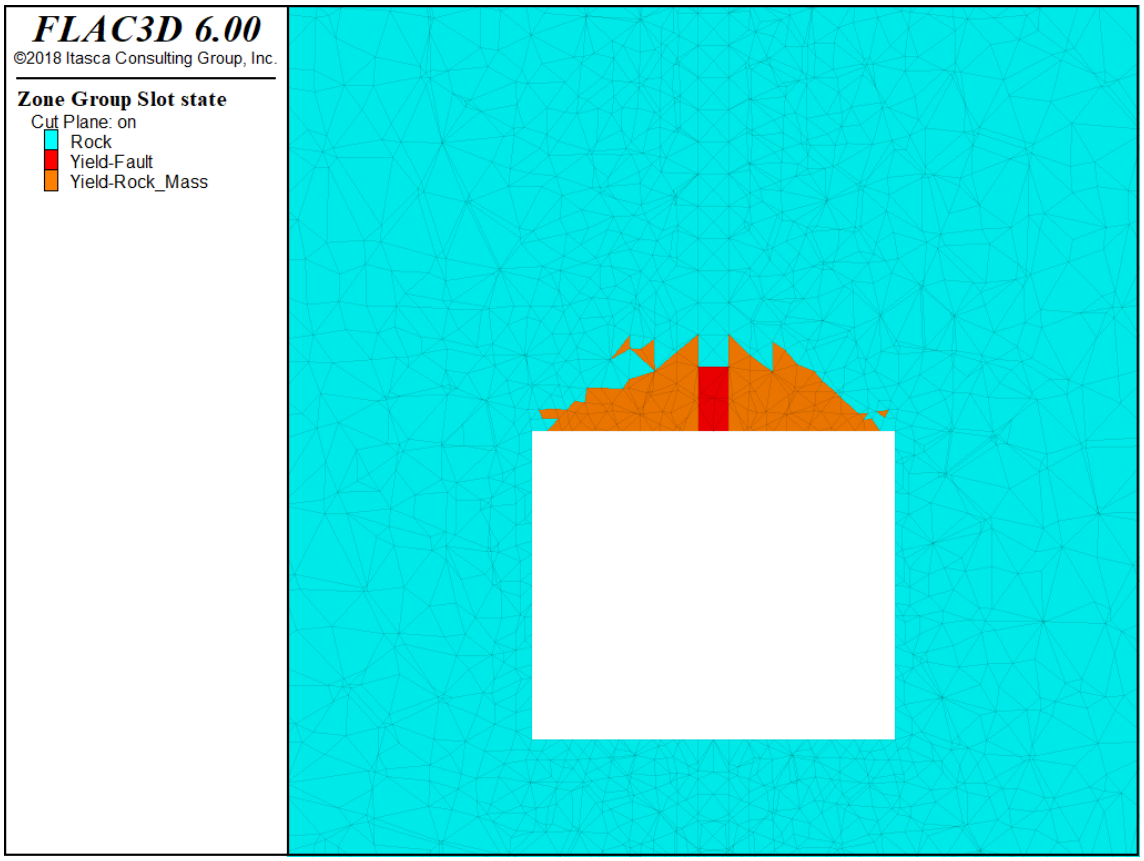

Figure 38 Strike 45, Dip 90 case mode

Strike 90°

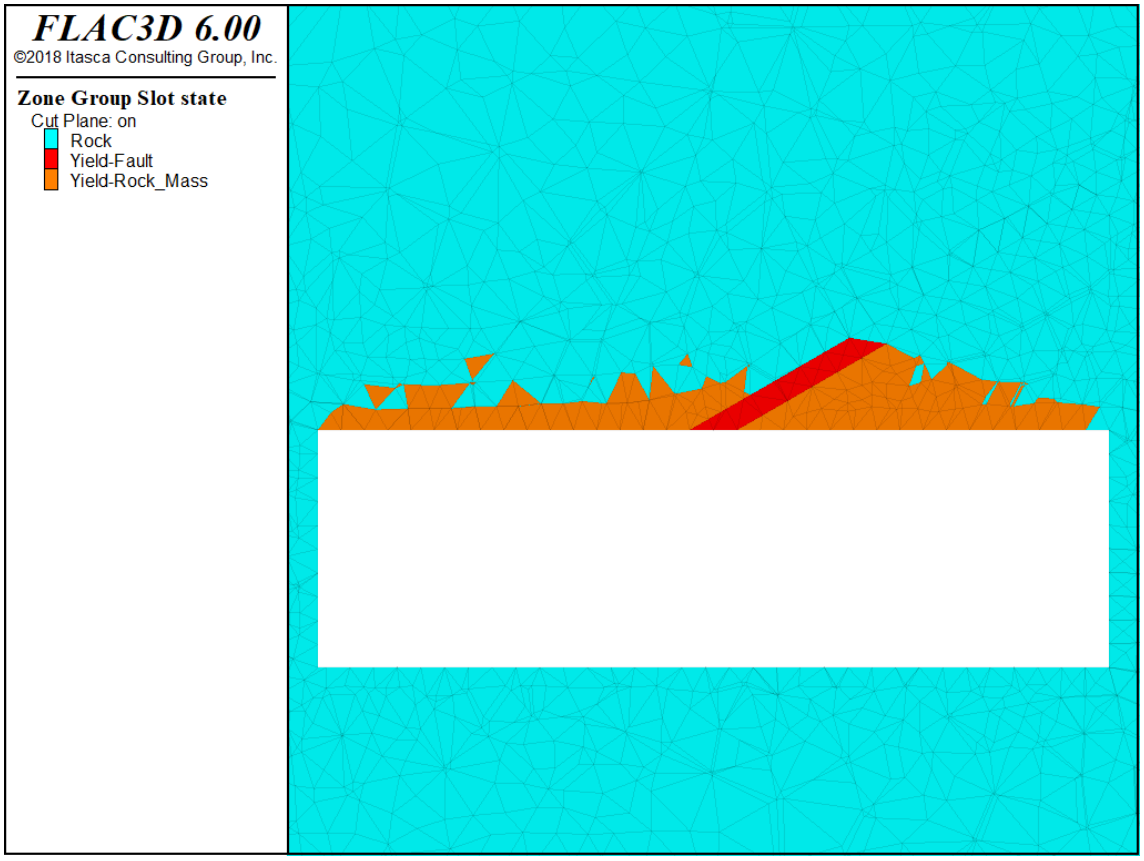

Figure 39 Strike 90, Dip 30 case model

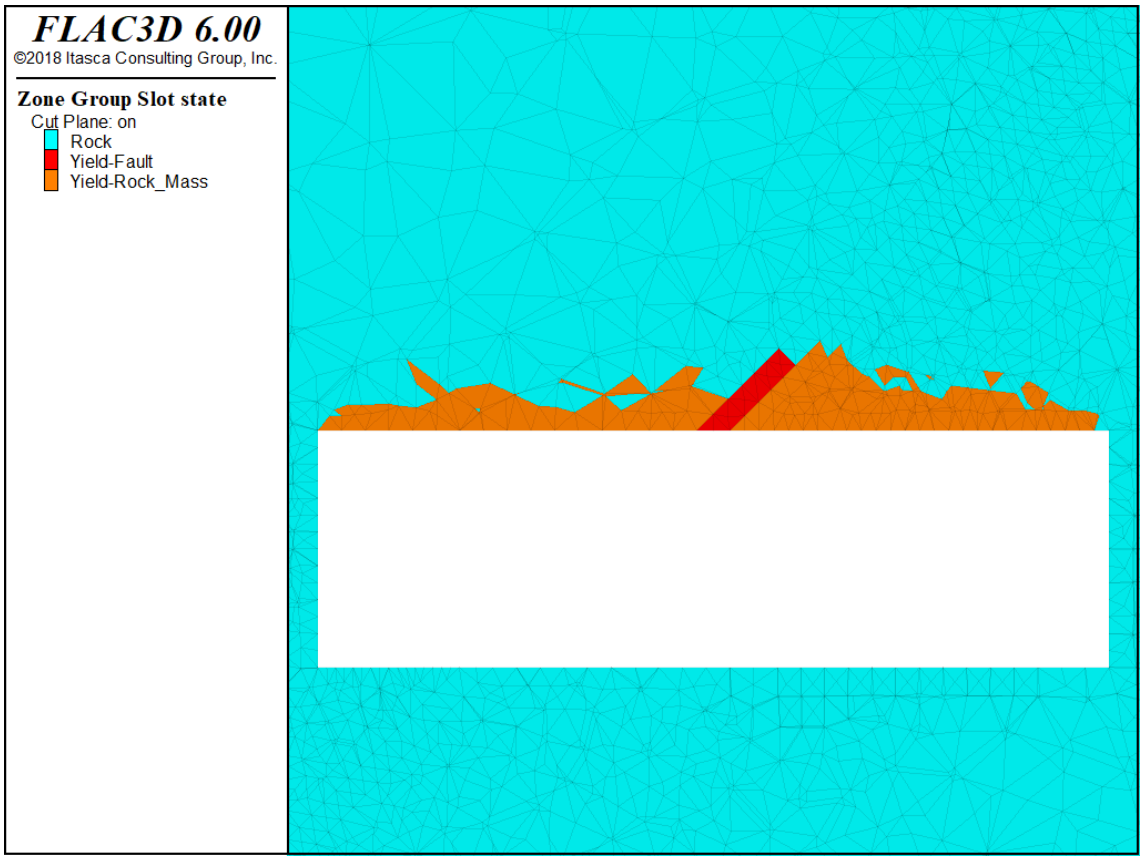

Figure 40 Strike 90, Dip 45 case model

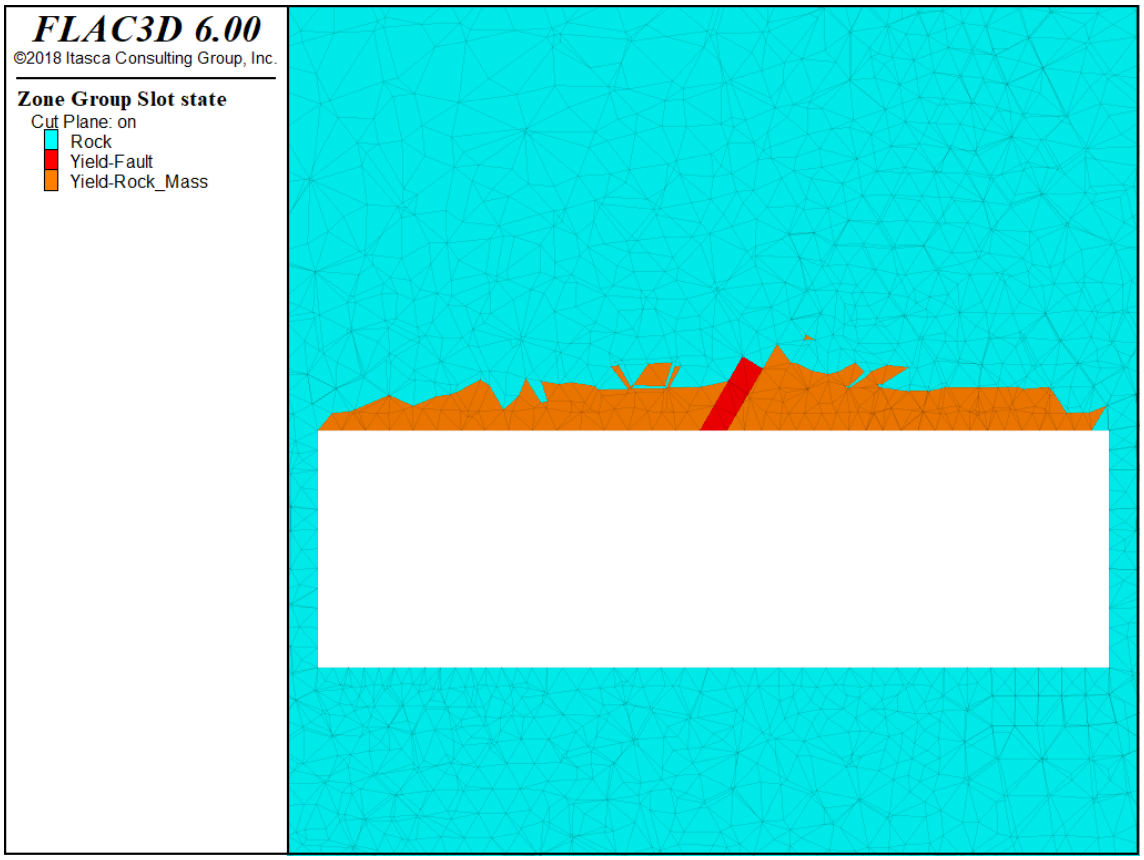

Figure 41 Strike 90, Dip 60 case model

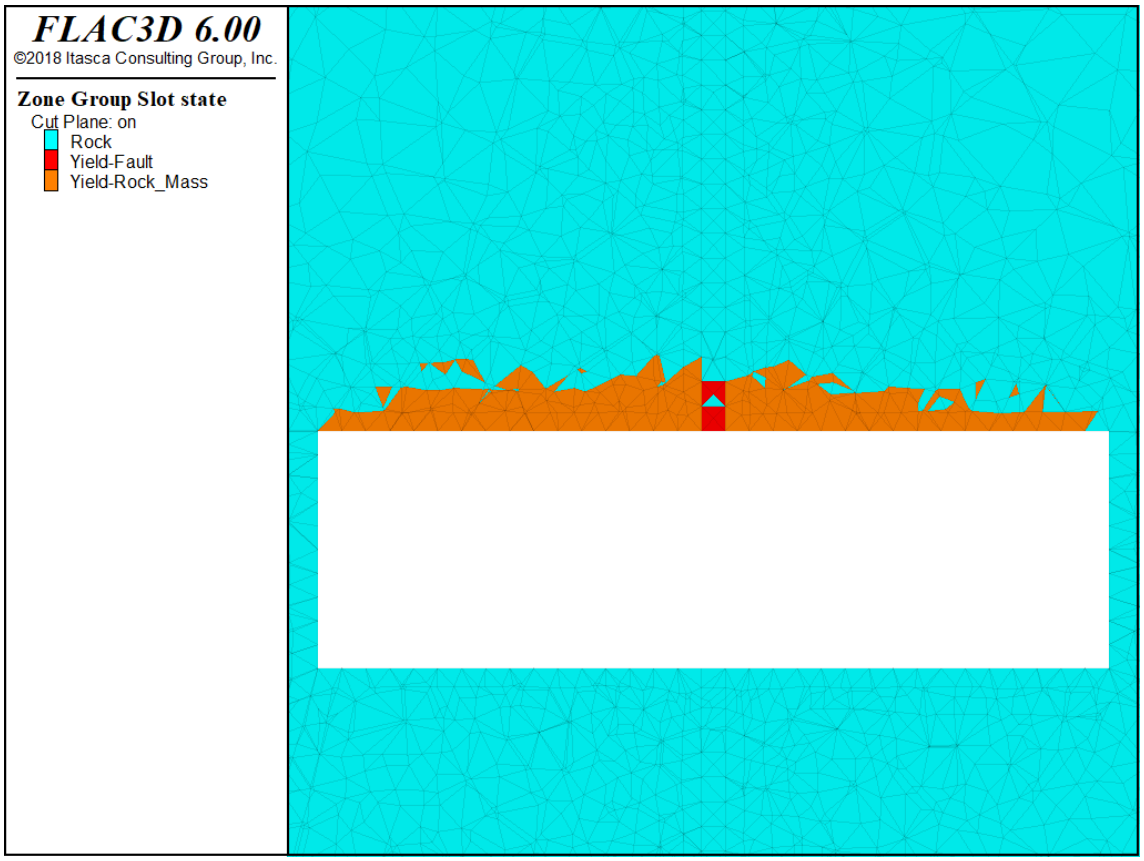

Figure 42 Strike 90, Dip 90 case model

Dip 0°

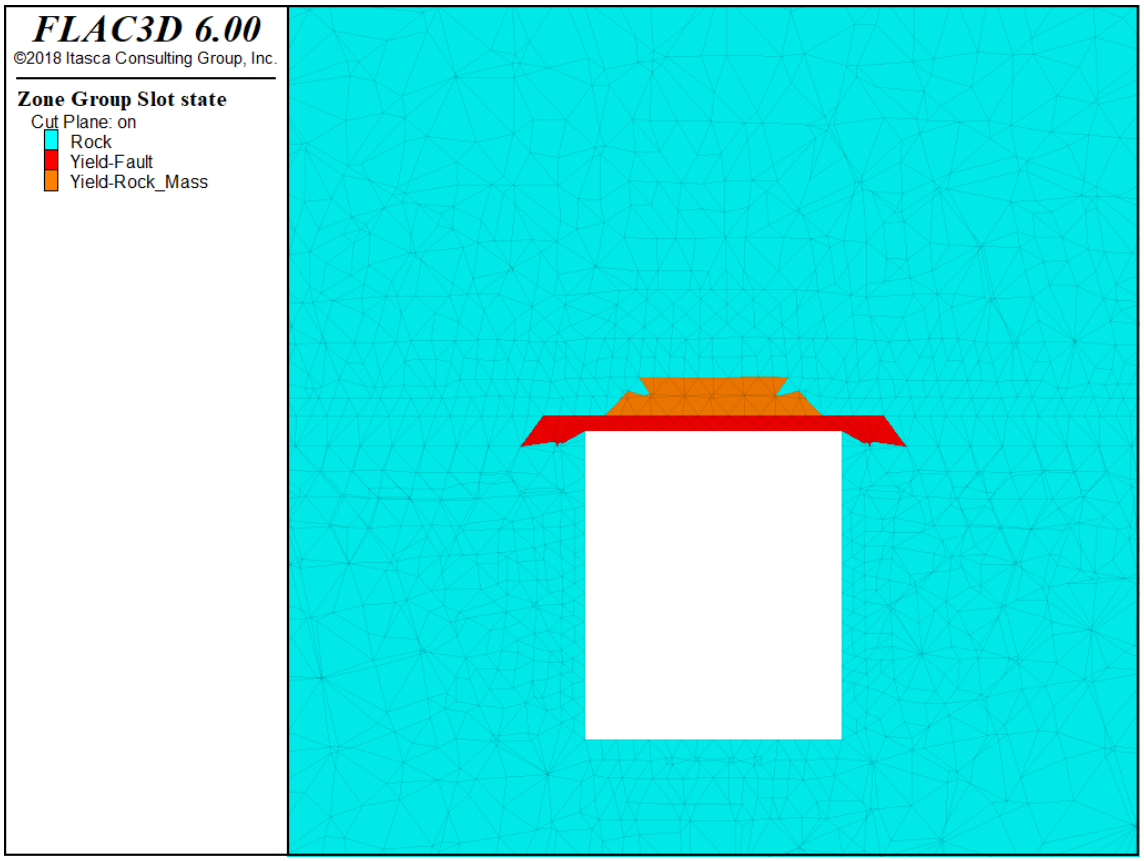

Figure 43 Dip 0 fault-back distance 0

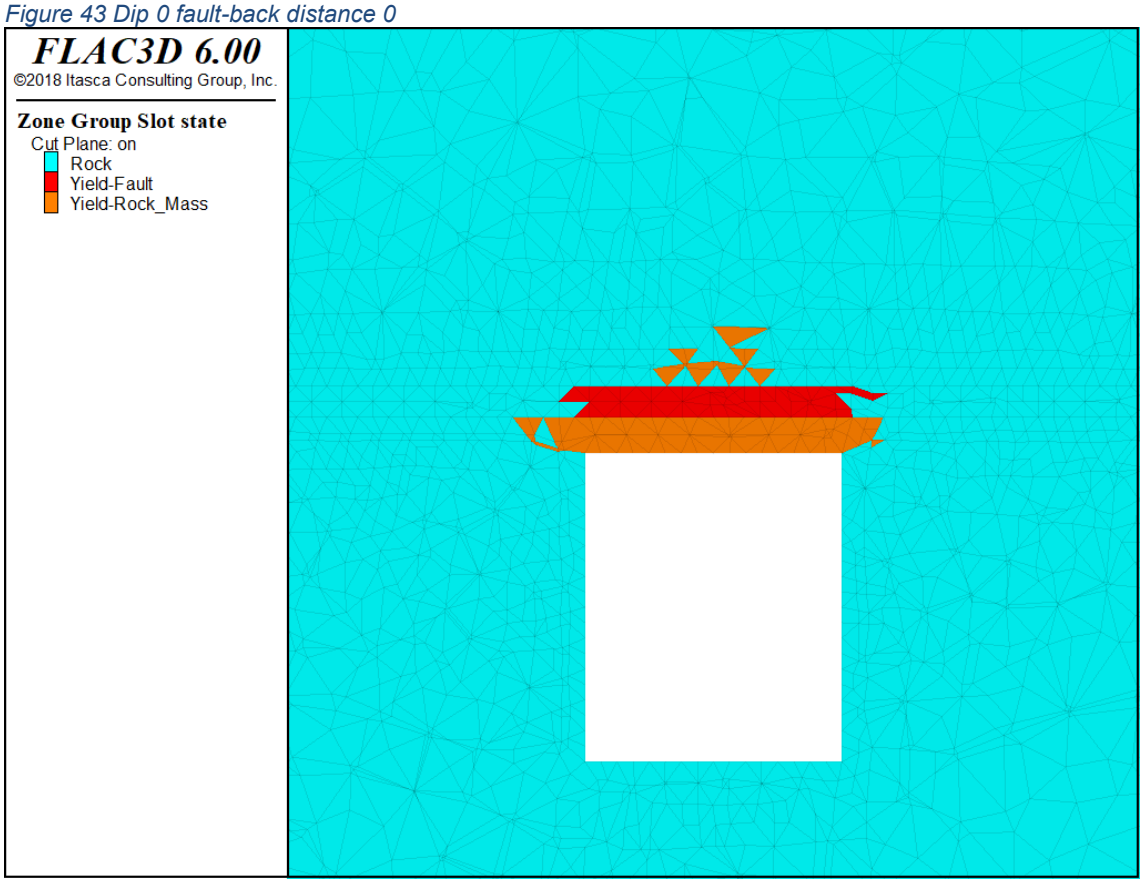

Figure 44 Dip 0 fault-back distance 5

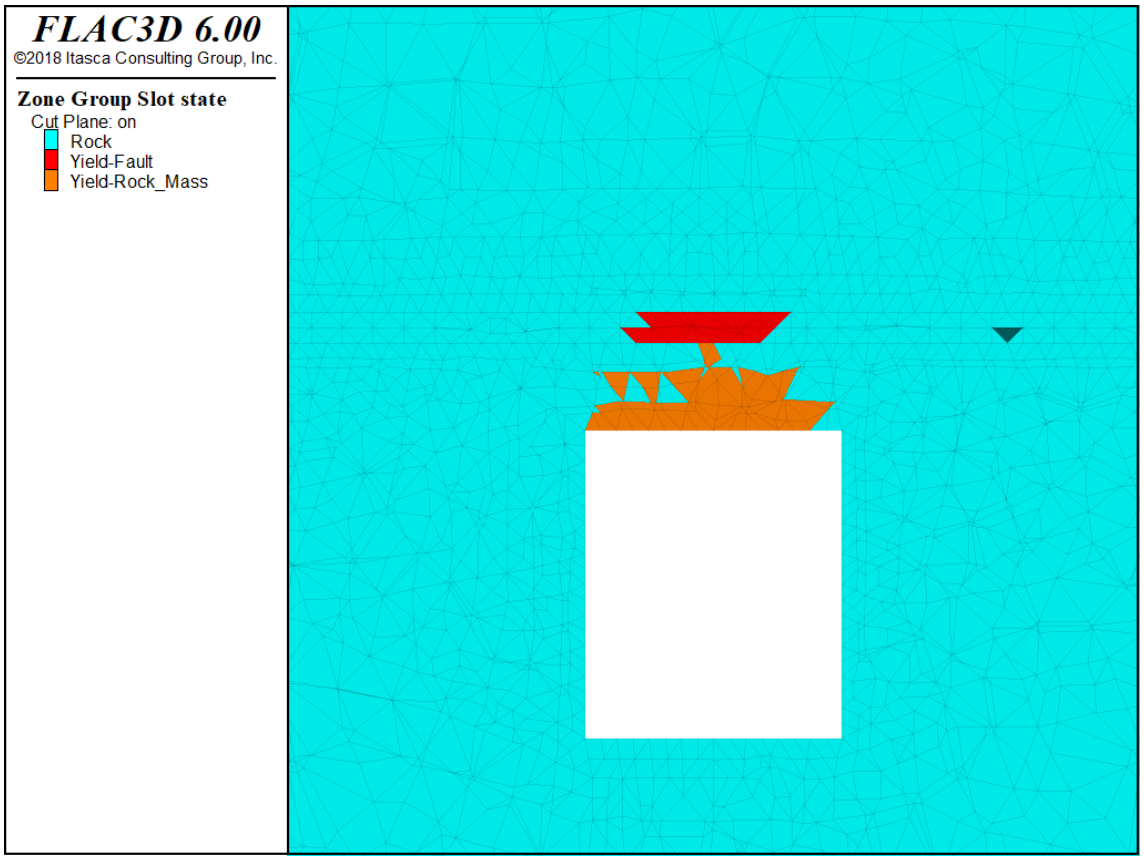

Figure 45 Dip 0 fault-back distance 10

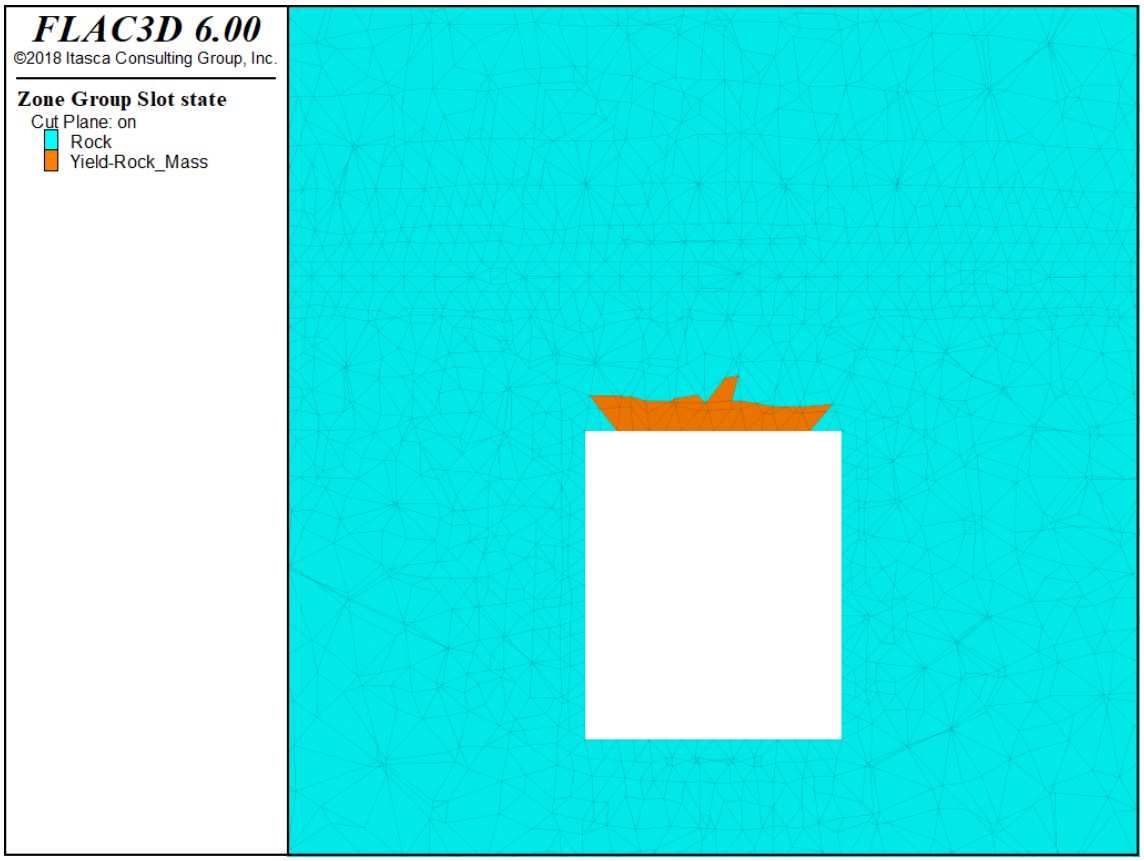

Figure 46 Dip 0 fault-back distance 15